

CHAPTER 3

Polarisation effects in optical fibres

The structure of this chapter is as follows. Section 3.1 discusses the single mode fibre operation condition and the electric field distribution of the fundamental mode in a cylindrical waveguide. Section 3.2 looks at the chromatic dispersion first, in general. The chromatic dispersion for S-SMF and DS step index fibre is computed and dispersion compensation is briefly discussed. The main focus of Section 3.3 is on the short length DGD which can be calculated from the local birefringence. The main origins of birefringences in standard telecommunication fibres are discussed which includes linear and twist induced circular birefringence, spun fibre is also considered. The birefringence and DGD due to one of the main internal birefringence effects of core ellipticity will be computed for different fibre parameters of common step index fibres. These results will be important for Chapter 6 when trying to understand the origin of the measured birefringence and DGD, and in Chapter 7 when trying to estimate the DGD from the measured birefringence at a single wavelength. There will also be discussion of the expected birefringence and DGD in fibres with more complicated profiles in the presence of core ellipticity and stress. Finally, in this section, the maximum allowed PMD in soliton systems using DEDF will be discussed (in Chapter 6 the measured DGD for different samples of DEDF will be shown). Section 3.4 considers the PMD in long lengths of fibres in the time domain and in the frequency domain. The frequency domain which is based on the eigenstate - principal state model will be the most important for us throughout this thesis because all our measurement results are based on this method. Measurement results on fibres with large differences in their PMD value will be shown and discussed. Section 3.5 reviews commercially available PMD measurement systems which can only measure on an end to end basis. Section 3.6 gives a short review of first order PMD and second order PMD in long lengths of fibres and a brief look into PMD compensation techniques.

3.1 *Single mode optical fibres*

The simplest fibre is step index fibre and its structure can be seen in Figure 3.1. The fibre consists of two different glasses which make a step function in their refractive index profile

to each other. The refractive index of the core must be higher than that of the cladding to guide the light in the core. The jacket around the core is for protection of the fibre from physical damage. The host material for low-loss optical fibres is silica glass and the refractive index difference between the core and cladding is normally realised by the inclusion of dopants in the core such as GeO_2 . The core-cladding index difference and radius of the core will be useful to determine the number of guided modes in the fibre. The relative index difference, Δ , between core- and cladding indices for step index fibre is

$$\Delta = \frac{n_1^2 - n_2^2}{2n_1^2} \approx \frac{n_1 - n_2}{n_1} = \frac{\Delta n}{n_1} \quad (3.1)$$

where n_1 is the refractive index of the core on the optical axis and n_2 the refractive index of cladding. The normalised frequency V which determines the number of modes in a fibre is defined for circular core step index fibre by

$$V = ak_0 \sqrt{(n_1^2 - n_2^2)} \quad (3.2)$$

where a is the core radius and k_0 is the free-space propagation constant. Optical fibres used for telecommunication are also called weakly guiding fibres because of the small refractive index difference $\Delta n \ll 1$. For the complete description of guided and radiated modes in perfectly round optical fibres, Maxwell's equations have to be solved for cylindrical geometry which can be found in standard books like [53], [54]. In weakly guiding fibres, it turns out that the higher modes cut-off when $V < 2.405$ so that only the fundamental mode in the fibre is supported [55]. The fundamental mode (HE_{11} mode) in single mode fibres does not have a cut-off wavelength like the higher modes and therefore exists at any wavelength and can be assumed to a good approximation to be a linearly polarised (LP_{01} mode) [55]. Rearranging Equation (3.2), the cutoff wavelength, λ_c , which is the minimum wavelength for single mode operation can be calculated

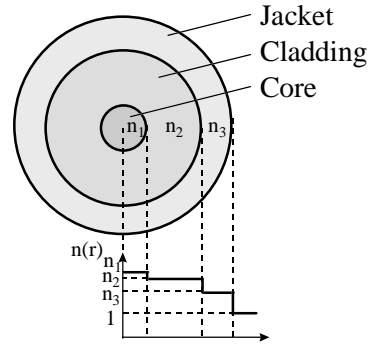


Figure 3.1 Cross section of step index single mode fibre with refractive index profile.

$$\lambda_c = \frac{2\pi}{V_c} a \sqrt{(n_1^2 - n_2^2)} = \frac{2\pi}{2.405} a \sqrt{(n_1^2 - n_2^2)} \quad (3.3)$$

The cutoff wavelength is an important parameter for single mode fibres and is recommended by the ITU-T to be around $\lambda_c = 1.2 \mu\text{m}$ for S-SMF which are designed for operation at $\lambda = 1.31 \mu\text{m}$ (see Appendix A). In a lossless fibre, assuming a monochromatic wave propagation in $+z$ direction, the electric field of the LP_{0l} mode can be written, similar to Equation 2.1, as two orthogonally polarised independent modes [53]

$$\vec{\mathbf{E}}(x, y, z, t) = \begin{bmatrix} F_x e_x^+ \\ F_y e_y^+ \end{bmatrix} e^{j(\omega t)} = \begin{bmatrix} F_x A_x e^{-j(\beta_x z + \phi_{x0})} \\ F_y A_y e^{-j(\beta_y z + \phi_{y0})} \end{bmatrix} e^{j(\omega t)} \quad (3.4)$$

where the subscripts x and y denotes the field direction, $F_{x,y}$ describes the spatial variation of the electric fields, $A_{x,y}$ the wave amplitudes, $\beta_{x,y} = 2\pi n_{x,y}/\lambda_0 = k_0 n_{x,y}$ the propagation constants for the effective indices $n_{x,y}$ of the fibre modes at the free space wavelength λ_0 , $\phi_{x,y}$ the initial phases of the electric fields and $\omega = 2\pi f$ is the circular frequency at the optical frequency f . The effective index for the x and y fields, n_{eff} , is, in general, somewhere between the indices of the core and cladding depending on the wavelength, and more primarily on the V value and index profile (Subsection 3.2.3). There are some more useful fibre parameters connected with the V value and n_{eff} which are the U and W parameters defined as

$$U = ak_0 \sqrt{(n_1^2 - \beta^2/k_0^2)} \quad \text{and} \quad W = ak_0 \sqrt{(\beta^2/k_0^2 - n_2^2)} = \sqrt{(V^2 - U^2)} \quad (3.5)$$

The electromagnetic field distribution $F_{x,y}$ of the LP_{0l} mode in a perfect circular step index fibre may be approximated by a Gaussian function [56]-[58]

$$F(r) = e^{-(x^2+y^2)/w_0^2} \quad (3.6)$$

where $F(r)$ denotes the unit amplitude field distribution of the fundamental mode with $r^2 = x^2 + y^2$ and w_0 the spot size or mode field radius which is the beam radius at the point $1/e^2$ of the centre intensity. Equation (3.6) describes an inhomogenous plane wave. For fibres with more complicated fibre structures, such as dispersion shifted fibres, the Gaussian beam approximation is still acceptable. The dependence of the spot size on the normalised V value

for ideal step-index single mode fibre is given within a fraction of a percent by the following empirical formula assuming a Gaussian beam [59]

$$w_0 = a(0.65 + 1.619/V^{3/2} + 2.879/V^6) \quad (3.7)$$

The spot size diameter (mode field diameter) for step index fibres at wavelengths longer than the cut-off wavelength is always larger than the core diameter. For S-SMF, after the ITU-T, the mode field diameter is recommended to be $2w_0 = 10 \pm 1 \mu\text{m}$. In general, the higher the V value, the smaller the w_0 value, and the field is better confined. Moreover, bending and micro-bending losses are decreased if operating near the cutoff wavelength.

3.2 *Chromatic dispersion*

This section provides a mathematical treatment of chromatic dispersion in a single mode fibre which originates from the wavelength dependence of the fibre propagation constant. Chromatic dispersion in single mode fibres is the net effect of material dispersion and waveguide dispersion. A simple simulation will be carried out to show the chromatic dispersion expected for S-SMF and DSF with step index profile where the chosen parameters for the simulated fibres and the discussion of different fibre structures relate especially to fibres from Corning and BT Labs. Measurement results of these fibres are shown in Chapter 6 and 7.

The attenuation of the pulse over long distances can be compensated through the use of optical amplifiers, hence, pulse spreading over distance limits the maximum distance for a given bit-rate. In an optical transmission system, dispersion may be grouped into linear and non-linear dispersion impairments. The linear are due to chromatic and polarisation mode dispersion whereas the non-linear are mainly due to self phase modulation. Chromatic dispersion has now been essentially overcome using dispersion shifted fibres together with dispersion management schemes [5], which can also keep the penalties due to non-linear effects within acceptable limits [6].

3.2.1 Material dispersion

The variation of the refractive index with wavelength in bulk optical materials is called material dispersion. The dependence of the refractive index of bulk silica with wavelength can be calculated by Sellmeiers dispersion equation [60] which basically considers just three resonance frequencies for the material. The values for the amplitudes and resonance frequencies can be found for doped and bulk silica in References such as [60] and [61].

3.2.2 Non-linear effects (Kerr effect)

The refractive index is not only a function of wavelength but also of the optical power, as evidenced by the non-linear Kerr effect. The non-linear component of the refractive index is, for typical power levels of 1 mW quite small compared to the linear component [46]. Despite this, the non-linear Kerr effect is still important in long-haul optically amplified systems where non-linear effects such as self phase modulation can accumulate over the entire span [46]. In soliton transmission, which has a high peak power value, the non-linear Kerr effect is used in a constructive sense to keep the shape of solitons due to an interplay between self phase modulation and chromatic dispersion.

3.2.3 Chromatic dispersion

The bandwidth of single mode fibres can be characterised in the time domain by pulse broadening which is determined by the spectral width of the pulse and the dispersion factors of the fibre. In high capacity systems, externally modulated narrow linewidth lasers are commonly used and the spectral width of the pulse is mainly determined by the bit-rate. Mathematically, fibre dispersion can be expressed by expanding the mode propagation constant, β , of the quasi monochromatic wave in a Taylor series around the centre frequency ω_0

$$\beta_i(\omega) \approx \beta(\omega_0) + \beta'(\omega_0)(\omega - \omega_0) + \frac{\beta''(\omega_0)}{2}(\omega - \omega_0)^2 + \frac{\beta'''(\omega_0)}{6}(\omega - \omega_0)^3 + \dots \quad (3.8)$$

where $\beta' = d\beta/d\omega$. The propagation constant β at a single frequency in a medium with effective index n_{eff} determines its phase velocity

$$v_p = \omega/\beta = c/n_{eff} \quad (3.9)$$

For the bandwidth in telecommunication systems, the group velocity, v_g , the speed with which the information of the modulated signal with spectral width $\Delta\lambda$ is travelling is of more importance and is given by

$$v_g = \beta'^{-1} = \frac{c}{n_g} = \frac{c}{n_{eff} - \lambda \frac{dn_{eff}}{d\lambda}} \quad (3.10)$$

where $n_g = n_{eff} + \omega \frac{dn_{eff}}{d\omega}$ is the group refractive index. The group transit time, τ_g , of the pulse travelling a distance, l , using Equation (3.10) is

$$\tau_g = l/v_g = l\beta' \quad (3.11)$$

Pulse spreading occurs because the components of the pulse arrive at different times depending on the group delay of their carrier wavelengths. The group velocity dispersion $d\tau_g/d\lambda$ defines the wavelength dependence of the group velocity which leads to the chromatic dispersion factor D

$$D = -\frac{1}{l} \frac{d\tau_g}{d\lambda} = -\frac{2\pi c}{\lambda^2} \beta'' \approx -\frac{1}{l} \frac{\Delta\tau_g}{\Delta\lambda} \quad \left(\frac{ps}{nm \cdot km} \right) \quad (3.12)$$

so that $\Delta\tau = -l \cdot \Delta\lambda \cdot D$ where $\Delta\lambda$ is the spread of the pulse in the wavelength domain and $\Delta\tau$ is the broadening of the pulse in the time domain. In the linear regime, operation at $\beta'' = 0$ is preferred but a signal will have spectral components that will experience dispersion on either side of the dispersion zero. The higher-order dispersion β''' gives the dispersion slope $S = dD/d\lambda$ which at $\beta'' = 0$ is

$$S_0 = -\frac{(2\pi c)^2}{\lambda^4} \beta''' \quad \left(\frac{ps}{nm^2 \cdot km} \right) \quad (3.13)$$

and the value for D for small wavelength range λ around $S_0(\lambda_0 \pm 25 \text{ nm})$ may be linearly approximated by

$$D(\lambda) = (\lambda - \lambda_0) S_0 \quad (3.14)$$

where λ is the operating wavelength. Chromatic dispersion (intramodal dispersion) defined in Equation (3.12) may be split into material dispersion, profile dispersion and waveguide dispersion as shown in Figure 3.2. Profile dispersion is normally treated as part of the waveguide dispersion in single mode fibres. In single mode fibres, the chromatic dispersion is normally the significant dispersion effect.

Chromatic dispersion is the net effect of *material dispersion* which is caused by the wavelength dependence of the fibre refractive index n_1 and n_2 , and *waveguide dispersion* which is caused by the wavelength dependence of the transverse field confinement defined by the spot size. At the typical operating conditions of $\lambda = 1.3$ and $1.55 \mu\text{m}$, the spot size extends into the cladding and the propagation of the mode is determined by the effective refractive index. Similar to the effective index, a normalised propagation constant can be defined as

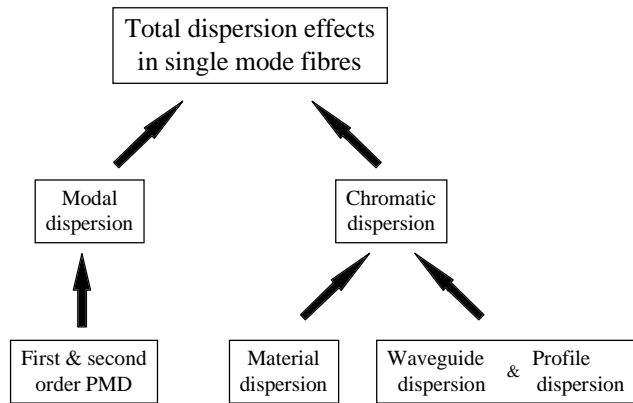


Figure 3.2 Linear dispersion effects in single mode optical fibres.

$$b_n(\lambda) = \frac{n_{eff}^2 - n_2^2}{n_1^2 - n_2^2} = 1 - \frac{U^2}{V^2} = \frac{W^2}{V^2} \quad (3.15)$$

In Figure 3.3, the normalised effective index for the fundamental LP_{01} mode is plotted for step index profile using Equation (3.15) together with the equation given in Reference [62] for W , which is obtained by a numerical finite element method. The relative error of W is given as smaller than 10^{-4} for $0 \leq V \leq 10$ which gives a maximum relative error for the normalised propagation constant of 0.3% for the step index profile and 0.7% for the parabolic profile for $V > 1.5$. In Figure 3.4(a), the total chromatic

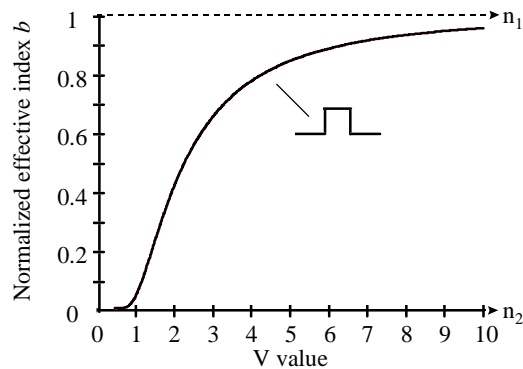


Figure 3.3 Frequency dependence of the normalised refractive index as a function of the V value for step index fibre.

dispersion for a single mode step index fibre and DS step index fibre with zero dispersion at $1.32 \mu\text{m}$ and $1.55 \mu\text{m}$ has been calculated numerically by evaluating the second derivative (Equation (3.12)) of the normalised propagation constant as shown in Figure 3.3 at a small difference in wavelengths.

The net chromatic dispersion in Figure 3.4(a) is mainly influenced by the material dispersion for the $1.3 \mu\text{m}$ designed step index fibre, and shifted by the waveguide dispersion for the $1.55 \mu\text{m}$ designed fibre. Operating the fibre at these wavelengths will minimise the effect of dispersion on optical pulse propagation. The region where D is negative is generally referred to as the normal dispersion regime and the positive regime is called the anomalous dispersion regime. For the chosen parameters of the step index fibre with core radius = $4.15 \mu\text{m}$ (Appendix A) and $\Delta = 0.28\%$, the necessary doping level of the core with GeO_2 using Equation (B.1), given in Appendix B, is $\sim 2.6 \text{ mol}\%$ which will be important in the next section when calculating the birefringence of the fibre. The other parameters obtained from the simulation are $\lambda_C = 1.18 \mu\text{m}$, $\lambda_0 = 1.32 \mu\text{m}$, $D(\lambda = 1.55 \mu\text{m}) = 15.6 \text{ ps/nm}\cdot\text{km}$, $w_0(\lambda = 1.3 \mu\text{m}) = 4.9 \mu\text{m}$, $w_0(\lambda = 1.55 \mu\text{m}) = 5.75 \mu\text{m}$ and $S_0 < 0.09 \text{ ps/nm}^2\cdot\text{km}$, which are within the ITU-T recommendation for single mode fibres given in Appendix A.

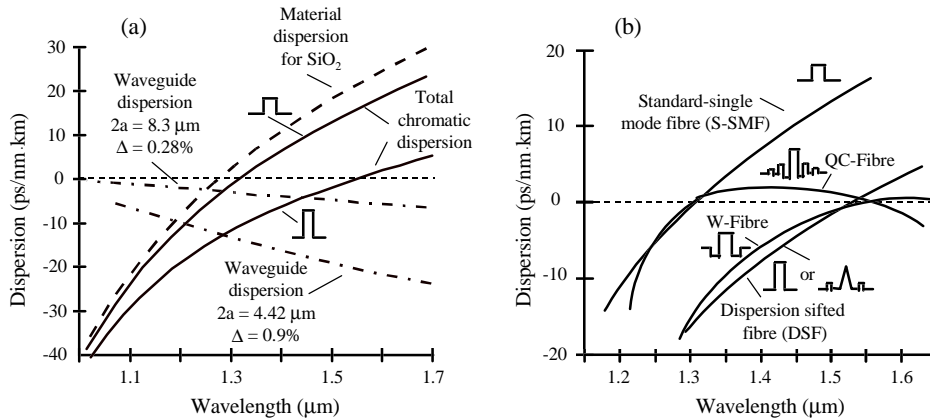


Figure 3.4 Calculation of the chromatic dispersion for (a) step index fibre, (b) and typical plot for chromatic dispersion of different fibre profiles, (From [63], [64])

The dispersion zero can be shifted by changing the fibre design, for example, changing the waveguide dispersion and cancelling of the material dispersion can be managed at one or more wavelengths [65]. For the dispersion shifted fibre in Figure 3.4(a), a step index approach has been used. For the chosen DS fibre with $\Delta = 0.9\%$ and $a = 2.21 \mu\text{m}$, the necessary doping level of the core with GeO_2 is $\sim 8.5 \text{ mol}\%$. The other parameters are $\lambda_C = 1.12 \mu\text{m}$, $\lambda_0 = 1.55 \mu\text{m}$, $w_0(\lambda = 1.55 \mu\text{m}) = 3.23 \mu\text{m}$ and $S_0 < 0.039 \text{ ps/nm}^2\cdot\text{km}$. In

general, this DS fibre design would work in the 1.55 μm window but there are some problems as the spot size is smaller than that recommended by ITU-T for DS fibre. Hence more energy travels in the cladding compared to step index fibre at 1.3 μm and therefore the bending loss is higher. Further, the dispersion zero is very sensitive to core diameter variations and the small size of the core radius makes handling of the fibre more difficult, e.g. expected higher splice losses. For DS fibres with step index profile, Δ has to be $> 0.4\%$ [66] and the core diameters have to be around $2a = 4.5 \mu\text{m}$. By using, for example, a parabolic profile, the zero dispersion at 1.55 μm with core diameters of about 6 μm can be obtained.

DS fibres with different profiles: Different modifications to the profile of the step index DS fibre have been suggested [63], [67] (see Figure 3.4(b)) to get a fibre whose zero dispersion wavelength is less sensitive to core variation and Δ . A sketch of the refractive index profile as patented by Corning fibre for its dispersion shifted fibre design with dispersion zero at 1.56 μm is shown in Figure A.1(b) (Appendix A). The relative refractive index difference Δ peak is as for the above simulated DS step index fibre at about 0.9% but the waveguide design is a two core segmented shape with a triangular core and an additional ring. Corning DS fibre specifications are given in Table A2 (Appendix A) as $\lambda_0 = 1.55 \mu\text{m}$ and with an inner core diameter of about 8 μm .

Different dispersion compensation techniques such as the use of dispersion compensating fibre or dispersion compensating gratings have been successfully demonstrated for some time [5], [68], [69] to convert existing 1.3 μm zero dispersion networks to dispersion flat fibre networks in the erbium window. This is only possible because chromatic dispersion is a deterministic characteristic of the fibre which is insensitive to changes in the environmental conditions. Hence, it is possible to predict accurately from factory measurement the compensation needed in advance for future installed systems and it is the main key to success in using dispersion compensation techniques in already installed systems. TAT12 designed to operate at 5 Gbit/s at a single wavelength is a good example of an advanced dispersion management system. For TAT12, short sections of S-SMF are installed to compensate for the dispersion of the DSF sections. In contrast, polarisation mode dispersion is inherently randomly varying with time and temperature, which makes compensation in general difficult if not impossible, and the best and obvious solution for controlled PMD is to ensure that all fibres (cables) have low and stable PMD.

3.3 *Birefringence effects*

The structure of this section is as follows. First, the local birefringence $\delta\beta$ and the related DGD due to the two local polarisation modes will be defined. We will also consider the short length DGD with units (ps/km) which is caused mainly by the internal birefringence of the fibre and is basically defined by the local birefringence. In Subsection 3.3.1, the two main effects for internal birefringence in low birefringent fibres, the geometrical asymmetry and stress field asymmetry [70], will be reviewed for S-SMF and DSFs. The DGD as a function of wavelength will be computed for these two birefringences. In addition, we will compute the phase velocity difference of the two polarisation modes at different frequencies in order to compare it with the DGD of the two modes. These comparisons will be more important for Chapter 7 when we try to estimate the DGD from the birefringence measured at a single frequency with a POTDR. Further, the circular birefringence due to twist will be reviewed while neglecting linear birefringence (as often carried out in literature), whereas in Chapter 5 we will derive the DGD due to linear and circular birefringence. Subsection 3.3.6 discusses the high birefringence and DGD in erbium doped fibres. The maximum acceptable PMD in soliton systems will be reviewed which will be interesting for Chapter 6 when we measure the DGD in DEDF which is a candidate for high speed soliton transmission.

3.3.1 *Birefringence origins in fibres and its dispersion*

A single-mode fibre can support two independent polarisation modes as introduced in Equation (3.4) which can be chosen arbitrarily orthogonal and all polarisation effects arise because of these two modes. In an ideal fibre, for example a perfect circular fibre, these two polarisation modes are degenerate and $\beta_x = \beta_y$. No polarisation effect will occur and any SOP launched into the fibre would propagate unchanged along the fibre. In real fibres this degeneracy is normally broken and fibre birefringence can result from either a geometrical deformation, stresses or various magneto-optic or electro-optic index changes.

In so called polarisation-preserving fibres, asymmetry is deliberately introduced in the fibre, for example, by a noncircularity in the core shape [71], stress lobes [72], [73] or by twisting to make high circular birefringence fibre [74]-[76]. High birefringent fibres exhibit, in general, a large PMD (see Figure 3.20(a)) which in theory could be reduced to low PMD by a combination of shape and stress birefringence as proposed in [77]. However, in ordinary telecommunication fibres, the SOP is, in general, not preserved and two modes may couple and exchange power due to fluctuation in the birefringence along the fibre. In such fibres, the

internal fibre birefringence $\delta\beta$ is mainly caused by a combination of core ellipticity (form birefringence) and an associated thermal stress anisotropy (stress birefringence). External stress birefringence or perturbation may be caused by bends, twists, handling etc.

In the presence of birefringence, the two modes in the fibre see different effective indices and travel now with different phase velocities. The difference between the effective indexes is best defined locally (if many birefringence effects co-exist) as the local birefringence

$$\delta\beta = (n_{eff,x} - n_{eff,y})k_0 = \beta_x - \beta_y \quad (3.16)$$

The birefringence causes the SOP to change along the fibre. In the absence of any extraneous coupling mechanisms a commonly used useful parameter, the beat length, can be defined as the length where the energy exchange from one polarisation mode to the other and back completes one cycle

$$L_b = 2\pi/\delta\beta \quad (3.17)$$

External perturbations with perturbation periods comparable with L_b can couple most efficiently energy from one polarisation mode to the other [78]. To avoid coupling, the value of L_b should be smaller than the perturbation periods which is the basic principle of polarisation maintaining fibres and modern spun fibres (Subsection 3.3.5).

The DGD or modal dispersion arises due to the difference in group delay of the two orthogonal polarisation eigenmodes (PEM) in the fibre. If the fibre polarisation matrix is independent of l (uniform fibre), then the two eigenvectors of the matrix which correspond to the polarisation eigenstates are independent of the optical frequency (Chapter 5). In a short fibre, the DGD increases linearly with length and has the units (ps/km). Using Equation (3.11), the local group transit time difference $\delta\tau$ per unit length is defined by the local birefringence vector which is, in general, elliptical on the Poincaré sphere as

$$DGD = \frac{\delta\tau}{l} = \frac{d(\beta_x)}{d\omega} - \frac{d(\beta_y)}{d\omega} = \frac{d(\delta\beta)}{d\omega} = -\frac{\lambda^2}{2\pi c} \frac{d(\delta\beta)}{d\lambda} = \frac{1}{c} \frac{d(\delta\beta)}{dk} \quad (3.18)$$

We may also define a differential phase delay (DPD) for a short length of fibre which is the phase transit time difference between the two polarisation modes at a single frequency

$$DPD = \frac{\delta\tau_p}{l} = \frac{\beta_x - \beta_y}{\omega} = \frac{\delta\beta}{\omega} \quad (3.19)$$

The relative difference in the DGD defined in Equation (3.18) from the DPD from Equation (3.19) at different centre frequencies may be calculated in general from

$$\Delta_\tau = 100 \frac{\delta\tau - \delta\tau_p}{\delta\tau} \% \quad (3.20)$$

In the following section, we will calculate Δ_τ for different birefringences and fibre types as a function of wavelength which will give an indication of the difference (error) when calculating the DGD from the birefringence at a single frequency (see Chapter 7, POTDR results).

3.3.2 Internal birefringence origins in fibres and its dispersion

The net birefringence in a fibre is normally caused by a combination of linear birefringence, $\delta\beta_L$, and circular birefringence, $\delta\beta_C$, effects due to, for example, shape-stress birefringence and twist, where the twist causes, in addition to the stress birefringence, a geometrical rotation. Locally, the net birefringence can be obtained by a simple vectorial addition [37], [79]. For shape $\delta\vec{\beta}_G$ and stress birefringence $\delta\vec{\beta}_S$ the resultant birefringence vector is given by [80]

$$\delta\vec{\beta} = \delta\vec{\beta}_G + \delta\vec{\beta}_S \quad (3.21)$$

In this thesis, the geometrical birefringence and stress birefringence are treated as a simple linear combination as carried out, in general, for low birefringent fibres [78], [81]. However, this artificial separation may lead to some discrepancies especially in highly elliptical fibres as believed in Reference [82]. The net birefringence of $\delta\vec{\beta}$ may be written in general, considering the geometrical mode factor in the fibre [78]

$$\delta\beta(\lambda) = bm(\lambda)C(\lambda)k_0 \quad (3.22)$$

where b is a frequency independent constant, $m(\lambda)$ is a geometrical mode factor describing the wavelength dependence of the confinement of the mode in the waveguide and

$$C(\lambda) = \frac{1}{2} n^3 (p_{11} - p_{12}) (1 + \nu_p) \frac{1}{E} \quad \left(\frac{\text{m}^2}{\text{kg}} \right) \quad (3.23)$$

is the stress optic coefficient for bulk fused silica with n the refractive index, p_{11} and p_{12} the components of the strain-optical tensor of the fibre material which are about 0.12 and 0.27 at $\lambda = 0.633 \mu\text{m}$ respectively [83], $\nu_p = 0.17$ the Poisson's ratio and $E \approx 7.45 \times 10^9 \text{ (kg/m}^2\text{)}$ [84] the Young's modulus for silica. The value for C is given in [84] for bulk silica as $C(0.633 \mu\text{m}) = -3.3 \times 10^{-11} \text{ m}^2/\text{kg}$. The weak frequency dependence of C arises mainly from some wavelength dependence of the photoelastic constants but also from the material dispersion of n as shown in Section 2.2. The chromatic dispersion characteristics of the stress-optical constant C shown in Figure 3.5 is calculated using the known dispersive law [84], [85]

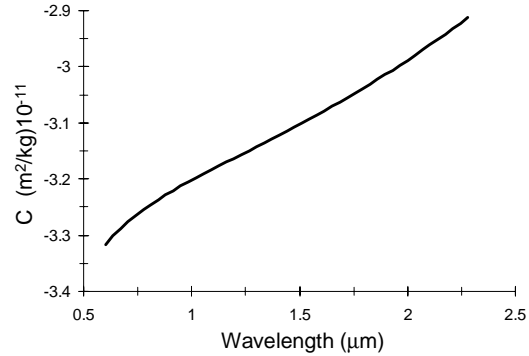


Figure 3.5 Wavelength dependence of the stress-optic coefficient.

$$C(\lambda) = C(\lambda_0) n(\lambda) \left(\frac{n(\lambda_0)}{n^2(\lambda)} \frac{\lambda^2}{\lambda_0^2} \frac{\lambda_0^2 - \lambda_1^2}{\lambda^2 - \lambda_1^2} \frac{\lambda^2 - \lambda_2^2}{\lambda_0^2 - \lambda_2^2} \right) \quad (3.24)$$

The dispersion of the net birefringence from Equation (3.22) is

$$\frac{\delta\tau}{l} = \frac{1}{c} \frac{d|\delta\beta|}{dk} = \frac{\delta\beta}{ck} + \frac{\delta\beta}{m} \frac{dm}{dk} + \frac{\delta\beta}{C} \frac{dC}{dk} \quad (3.25)$$

3.3.2.1 Form birefringence $\delta\beta_G$ due to geometrical anisotropy

In this subsection, the wavelength dependence and magnitudes of the main birefringence effects in standard telecommunication fibres which contribute to the PMD will be considered. These are shape, stress and twist induced birefringence. The simulation results for the stress birefringence are mainly concerned with the available Corning S-SMF used in the experiments (Chapter 6 and 7) which has an undoped cladding. From the step index, simulation results for birefringence and dispersion, the expected values for fibres with more complex profiles, such as, the segmented DSF design of Corning, or the triangular profile DSF of BT labs, will be discussed.

Form birefringence (shape birefringence) is basically caused by an elliptical core, the refractive index distribution deviates from rotational symmetry and introduces a linear birefringence in the fibre with fast axis along the minor axis. For just form birefringence, the stress optic coefficient C in Equation (3.22) is equal to one. In the real world, the cross section of the fibre core cannot be expected to be perfectly circular and will always have some deviation from it as indicated in Figure 3.6. For example, in the MCVD technique, fibre ellipticity originates mainly from the expected noncircularity in the silica tube [86] which gets impressed in the fibre core - cladding after collapsing the tube (Appendix B). One of the simplest deviations from a circular shape of the core is to assume an elliptical deformation of the refractive index profile of the core. The resulting perturbation is a scalar described just by the radial co-ordinates of the fibre. For a step index fibre with elliptical core, the ellipticity parameter, e , may be defined as

$$e^2 = 1 - b^2/a^2 \quad (3.26)$$

where b and a are the minor and major half axes of the elliptical core respectively as shown in Figure 3.6. For small ellipticities, e^2 is sometimes expressed as $e^2 \approx 2(1 - b/a)$ or by the fibre ovality $e \approx 2O$ with $O = 2(a - b)/(a + b)$. For specific core shapes and index profiles, different methods of varying accuracy and simplicity for calculating the form birefringence have appeared in the literature, such as using coupled mode theory, vector perturbation theory or a finite element formulation for solving Maxwell's equation [87], [88]. Although the finite element is powerful for solving arbitrary fibre profiles [82], [89], the perturbation theory given by Sammut [90], assuming weak guidance and small ellipticity, is adequate to describe the shape birefringence in step index telecommunication fibres, [90]-[92],

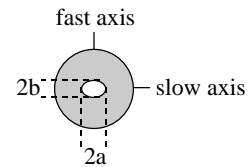


Figure 3.6 Elliptical core

$$\delta\beta_G = \frac{1}{a} e^2 (2\Delta)^{3/2} \delta\beta_G^* \quad (3.27)$$

with $\delta\beta_G^*$ the normalised birefringence

$$\delta\beta_G^* = \frac{U^2 W^2}{8V^3} \left(1 - \frac{J_0^2(U)}{J_1^2(U)} \left(1 - \frac{W^2}{U^2} + \frac{W^2 J_0(U)}{U J_1(U)} \right) \right)$$

where $J_{0,1}$ are Bessel functions of the first kind (of zeroth and first order). The shape birefringence in Equation (3.27) depends strongly on the frequency or V value. In Figure 3.7(a), a sketch of $\delta\beta_G^*$ as a function of the V value for step index, parabola and triangle profile is shown. The maximum birefringence introduced by the elliptical core decreases as the profile moves away from a perfect step index. The lines on the curves in Figure 3.7(a) specify the cut-off frequencies for the different profiles which occurs at about the maximum birefringence [92], [93].

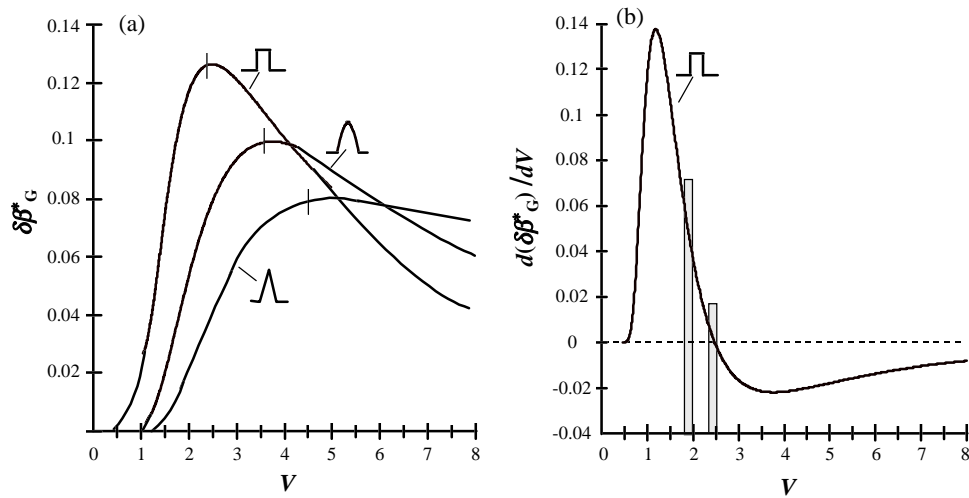


Figure 3.7 In (a) Sketch of normalised phase difference $\delta\beta_G^*$ as a function of V for different profiles, (From [92]). In (b) simulation of $d(\delta\beta_G^*)/dV$ as a function of V for step index profile.

For ellipticities smaller than 10% the accuracy of Equation (3.27), as given in [91], is better than 5%. The ellipticities for typical communication-grade fibres are fairly small, $e < 2.5\%$ [81], which we could also confirm for the majority of fibres for which we have investigated the ellipticity and birefringence (Chapter 6 and Appendix C). For fibres with larger ellipticities as, e.g. in some high birefringent fibres second order corrections for the phase difference are given in [91], [92]. For increasing ellipticities the higher mode cut-off decreases to smaller V values compared to the ones indicated in Figure 3.7(a) for the three different profiles [93]. The central refractive index which often dips in real fibres shifts the maximum birefringence to higher V but reduces the magnitude of the overall birefringence [81], [92]. The group velocity dispersion due to the shape birefringence given in Equation (3.27) can be obtained by using Equation (3.18) as

$$DGD = \frac{\delta\tau}{l} = \frac{n_1 e^2 (2\Delta)^2}{a} \frac{\delta\beta_G^*}{dV} \quad (3.28)$$

where the material dispersion has been neglected. Figure 3.7(b) represents the computed dispersion of the normalised shape birefringence as a function of V . The zero crossing of the curve in Figure 3.7(b) is close to the higher mode cut-off condition at $V = 2.4$. For this reason at $1.3 \mu\text{m}$, which is close to $V = 2.4$, the DGD due to shape birefringence is normally negligible for small Δ and core ellipticities, and the thermal stress birefringence as treated afterwards is dominant. The V value at $\lambda = 1.55 \mu\text{m}$ is $V \approx 1.9$ where the shape induced dispersion is no longer zero and must be considered in step index fibres, especially in DS step index fibres.

In Figure 3.8(a) the DGD for increasing ellipticity in the wavelength range of interest has been computed, including the material dispersion $n(\lambda)$ where Δ and the core diameter are nominal values as expected for standard step index fibres (see Appendix A Corning fibres and ITU-T recommendation for S-SMFs).

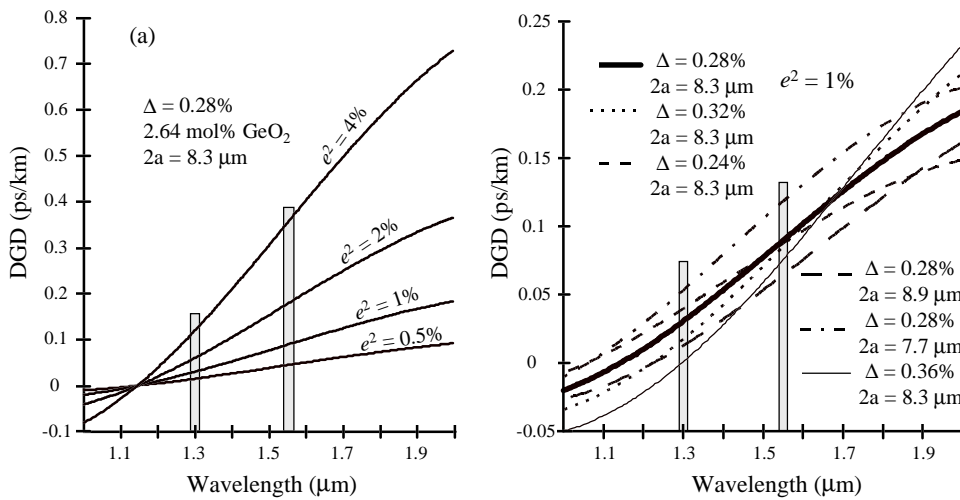


Figure 3.8 Simulation of the DGD due to shape birefringence, $n(\lambda)$ is considered (a) for increasing ellipticities, (b) S-SMF with allowed minimum and maximum values for Δ and a given by the tolerances specified by ITU-T for w and λ_C .

The DGD in Figure 3.8(a) increases linearly with increasing ellipticity as expected from Equation (3.28). If the material dispersion is neglected in this wavelength range the error in the DGD is $< 2\%$. Figure 3.8(b) shows the DGD due to the shape birefringence for 1%

ellipticity with the minimum and maximum allowed deviations of the core radius and Δ around the nominal value ($\sim 10\%$) used in Figure 3.8(a) after ITU-T recommendation. The minimum and maximum deviation of a and Δ are defined by the allowed deviation of the mode field diameter w_0 and cut-off wavelength λ_c in S-SMF after ITU-T (see Appendix A). There is also a plot in Figure 3.8(b) for $2a = 8.3 \mu\text{m}$ and $\Delta = 0.36\%$ which are the specified values for the Corning step index fibre as given in Appendix A, which give a cut-off wavelength slightly above the higher λ_c recommended by ITU-T, but which may be shifted to a lower cut-off in a real fibre due to the expected deviation from the ideal step index profile.

The DGD of the shape birefringence in step index DS fibre with zero dispersion at $1.55 \mu\text{m}$ is shown in Figure 3.9(a), with the same ellipticities as for the S-SMF in Figure 3.8(a). The DGD is about an order of magnitude higher for the chosen Δ and core radius as would be expected from Equation (3.28). In Figure 3.9(b) step index DSFs with less core doping have been chosen and the DGD could be reduced by a factor of two, but the core radius is still small compared to the S-SMF.

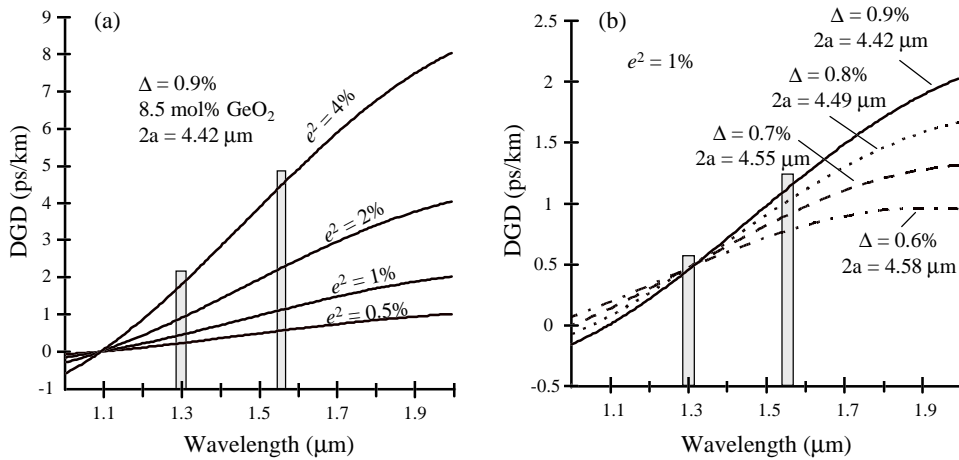


Figure 3.9 Simulation of the DGD due to shape birefringence for DS step index fibre, considering material dispersion.

The relative refractive index difference in Figure 3.9(a) was chosen as $\Delta = 0.9\%$ which is about the same magnitude as the peak value for the segmented DSF from Corning, Figure 3.10(a). It can be said, in general, that for fibres with more smoothly changing profiles than the step index profile, e.g. parabolic profile or triangular profile like the Corning fibre, the chromatic dispersion is less sensitive to core diameter variations. Another advantage of the smoothly changing refractive index of the triangular core shaped DSF is, as expected from

Figure 3.7(a) the smaller birefringence and hence the smaller DGD as shown for the segmented DSF from Corning in Figure 3.10(b).

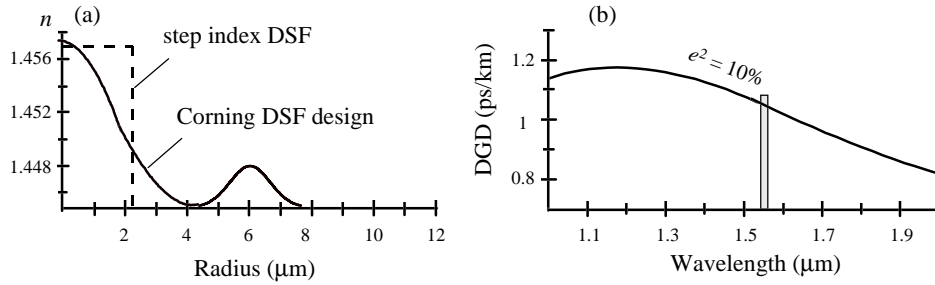


Figure 3.10 DGD of a segmented dispersion shifted fibre with 10% ellipticity (From [88]).

3.3.2.2 Stress birefringence $\delta\beta_s$ due to material anisotropy

Linear birefringence due to stress may have internal or external origin. Internally the stress may be caused by the ellipticity of the core itself which causes asymmetrical residual stress in the fibre due to the thermal expansion mismatch between the doped core and cladding. [94] [95]. Externally the stress may be due to applied pressure, fibre bends [78] with axial tension [96] or due to cabling [97]. In Chapter 6 the fibre DGD due to externally applied uniaxial pressure will be investigated. The birefringence due to internal thermal stress anisotropy, which develops during drawing when the fibre cools through the temperature at which the glass sets, can be expressed as [98] [99]

$$\delta\beta_s = \frac{EC}{(1-\nu_p)} (\alpha_1 - \alpha_2) \Delta T b_n(\lambda) k_0 \frac{1}{2} O \quad (3.29)$$

where α_1 and α_2 are the temperature expansion coefficients of the core and cladding material respectively, and ΔT the difference between the glass softening temperature and room temperature. The stress birefringence $\delta\beta_s$ in Equation (3.29) is proportional to the core ellipticity and depends on the electric field distribution indicated by the normalised propagation constant, which is mainly due to a direction dependent stress change in the core-cladding interface which arises from the thermal expansion mismatch between the core and cladding [98] [99]. The temperature expansion coefficient is a linear function of the refractive index and doping level, provided that the doping concentration g_q , is small, and can be estimated at low temperatures [94]

$$\alpha_{q+SiO_2} = g_q \alpha_q + (1-g_q) \alpha_{SiO_2} \quad (3.30)$$

where α_q is the thermal expansion coefficient, whose values at low temperatures can be found for fused silica and some of the often used codopants [94], [83]

$\text{SiO}_2 \approx 0.55 \times 10^{-6} \text{ C}^{-1}$	$\text{P}_2\text{O}_5 \approx 14 \times 10^{-6} \text{ C}^{-1}$
$\text{GeO}_2 \approx 7 \times 10^{-6} \text{ C}^{-1}$	$\text{Al}_2\text{O}_3 \approx 5.9 \times 10^{-6} \text{ C}^{-1}$
$\text{B}_2\text{O}_3 \approx 10 \times 10^{-6} \text{ C}^{-1}$	

Table 3.1 Thermal expansion coefficients for silica and some of its dopants.

The temperature difference ΔT between the softening temperature and the room temperature depends mainly on the type of glass. The fibres we have measured are doped differently. The fibres from Corning (&Optical Fibres) are only Ge-doped in the core [100], whereas the fibres from BT Labs are Ge-doped in the core and Phosphor - Fluoride doped in the cladding [86]. Reference [94] estimates the ΔT -values of Ge-doped and P-doped silica at 1000 and 1100 °C respectively, and calls the value “conservatively low”. No value is specified for the Al-doped silica used in EDF and F-doped silica, but it will be in any case lower than the value for pure silica which is ≈ 1500 °C. According to [101] the linear approximation of the thermal expansion coefficient seems to underestimate the birefringence by a factor of 1.6 and it is suggested that one would better change the factor $(\alpha_1 - \alpha_2) \Delta T$ to the integral $\int (\alpha_1 - \alpha_2) dT$.

3.3.2.3 Simulation results for shape and stress birefringence

In the simulation below the fibre parameters for the Corning S-SMF fibre have been used with Ge-doped core and pure Silica in the cladding. The softening temperature ΔT has been taken as 1000 °C, the thermal expansion coefficients are calculated from Equation (3.30) and the values given in Table 3.1. The direction of the fast axes of the stress-induced birefringence depends on the sign of the thermal expansion coefficient difference of core and cladding. For the doped elliptical core surrounded by the pure silica cladding, the fast axis is parallel to the minor axis of the ellipse, $\delta\beta_G$ and $\delta\beta_S$ have the same sign and the internal birefringence increases [98] [99].

In Figure 3.11(a) the birefringence due to shape and the corresponding thermal stress birefringence for the expected nominal values of S-SMF (Corning) are plotted for different fibre ellipticities as a function of the V value using Equation (3.29) and Equation (3.27). It

can be seen that in the interesting V range from 1.8 to 2.4 the stress birefringence, especially for higher ellipticities and larger V values, dominates over the shape birefringence. The combined effect of the stress and shape birefringence given by Equation (3.21) is simply the addition of both birefringences for the doped core, and the resultant birefringence is shown in Figure 3.11(b).

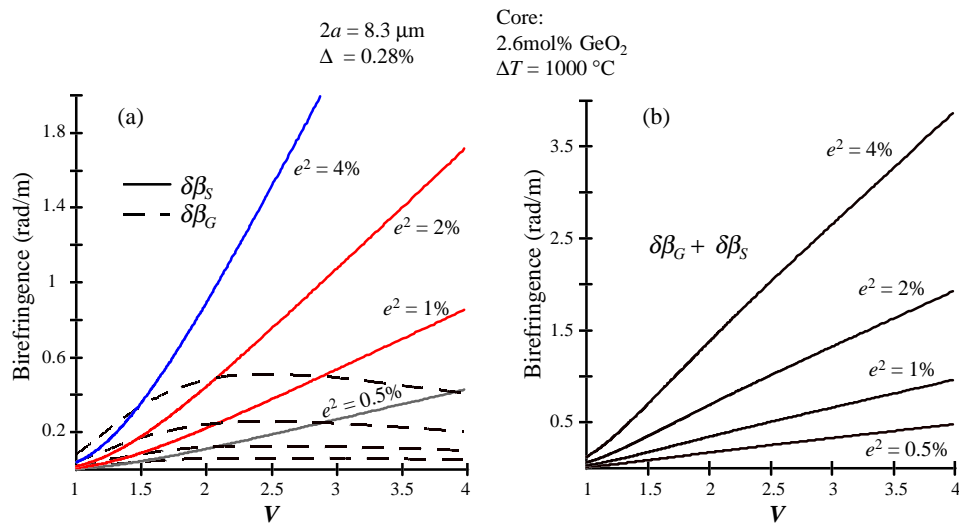


Figure 3.11 Simulation of $\delta\beta_G$ and $\delta\beta_S$ as a function of the V value for different core ellipticities, with $C(\lambda)$ and $n(\lambda)$.

The effects on the birefringence with values around the nominal value for the core diameter and refractive index difference, as used for the S-SMF in Figure 3.11 with 1% ellipticity are shown in Figure 3.12(a) and (b). The deviation of the net birefringence from the nominal value in Figure 3.12(b) (centre line) is about $\pm 20\%$, as a result of the $\sim 10\%$ allowed deviation of spot size and zero dispersion wavelength allowed by ITU-T recommendation (Appendix A). For DS step index fibre in Figure 3.13(a) and (b) the birefringence of $\delta\beta_G$ and $\delta\beta_S$ is plotted in the same way as in Figure 3.11(a) and (b), the interesting result is that now the shape birefringence is dominant in the V range from 1.8 to 2.4 because of the much stronger effect of Δ and the core radius on $\delta\beta_S$.

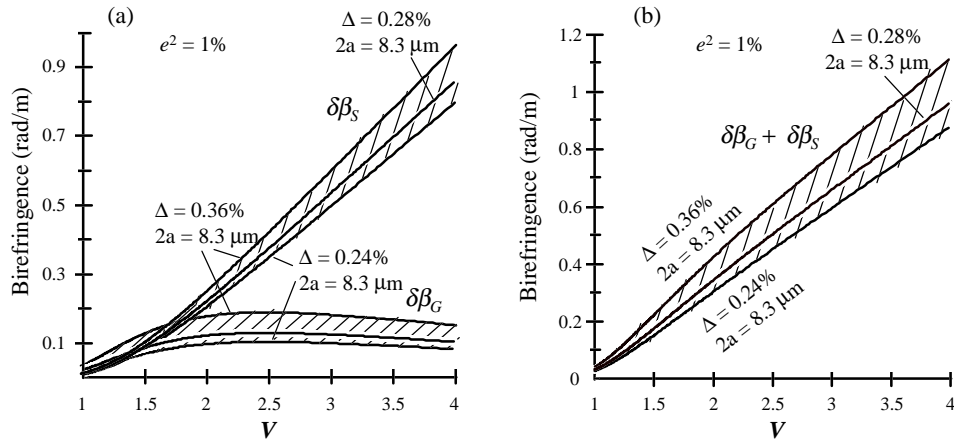


Figure 3.12 Simulation of $\delta\beta_G$ and $\delta\beta_S$ as a function of the V value for 1% core ellipticity, with $C(\lambda)$ and $n(\lambda)$.

From the net birefringences in Figure 3.11(b) and Figure 3.13(b) it is possible to calculate the DGD from Equation (3.18) by computing the differential numerically with a small wavelength step size and the DPD at a single frequency using Equation (3.19).

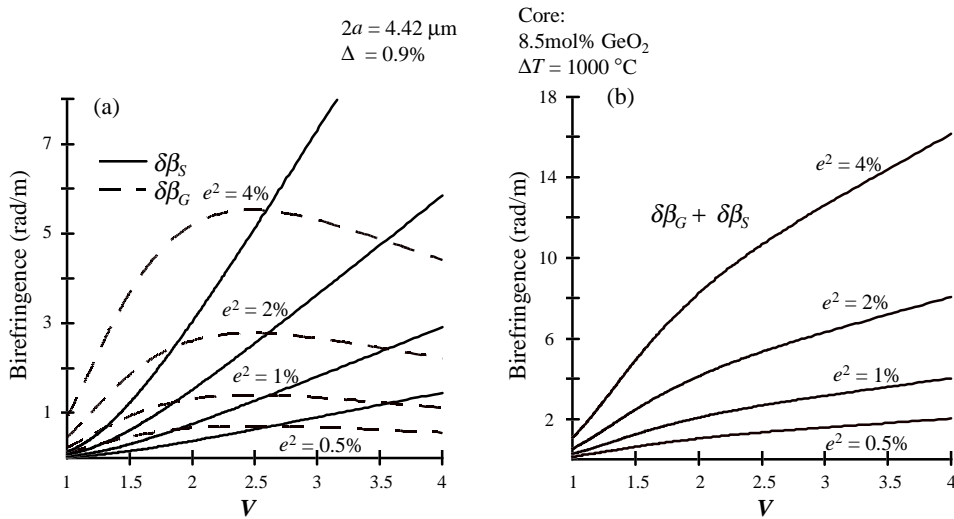


Figure 3.13 Simulation of $\delta\beta_G$ and $\delta\beta_S$ for elliptical step index DSF as a function of the V value for different core ellipticities, with $C(\lambda)$ and $n(\lambda)$.

In Figure 3.14(a) the calculated DGD and DPD are plotted for the birefringence of the S-SMF in Figure 3.11(b). The solid line in Figure 3.14(a) corresponds to the DGD which is nearly constant over the wavelength range from 1 to 2 μm at the different ellipticities. The dashed line in Figure 3.14(a) shows the DPD for the different fibre ellipticities where it can be seen that there is quite a large offset between the DGD and DPD. The relative difference Δ_r of the DGD and DPD is plotted in Figure 3.14(b) as a function of wavelength at the different

ellipticities. It is very interesting to see that for the plotted ellipticities the offsets in Δ_τ is smaller than 0.5%, nearly the same line for all the ellipticities, which will be important in Chapter 7 when we try to estimate the DGD from the measured fibre birefringence by knowing the fibre profile.

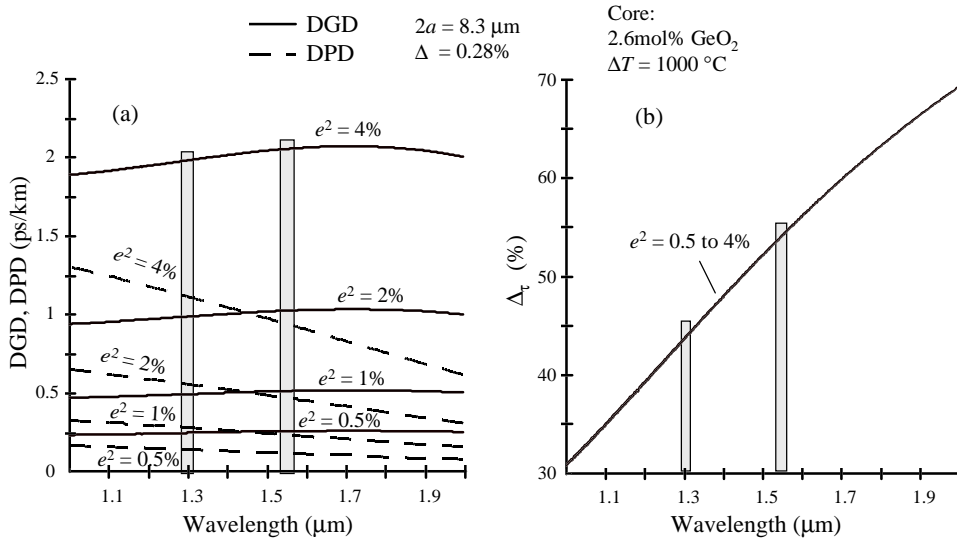


Figure 3.14 S-SMF (a) DGD and DPD due to $\delta\beta_G + \delta\beta_S$ for different core ellipticities (b) relative difference in DGD and DPD.

A more realistic picture of the expected DGD and DPD is shown in Figure 3.15(a), where the DGD and DPD is plotted for an allowed deviation of the fibre parameters Δ and a in the same way as used in Figure 3.12 for the birefringence. The DGD in Figure 3.15(a) varies by about 20% around the DGD, calculated from the nominal fibre values which also indicates that in fibres with the same ellipticity a DGD fluctuation in this range is very likely. The minimum and maximum difference in the DGD and DPD in Figure 3.15(b) is between 40% and 60% at 1.55 μm for the different simulated fibre parameters.

Figure 3.16(a) shows the DGD and DPD due to shape and stress birefringence for the step index DS fibre for increasing core ellipticity. The DS fibre in Figure 3.16(a) is, as expected, more sensitive to core ellipticity in the DGD value than the S-SMF with similar ellipticities shown in Figure 3.14(a), which is because of the higher index difference and smaller core diameter. In the step index DS fibres, shape and thermal stress birefringence make approximately equal contributions to the intrinsic DGD (compare Figure 3.16(a) with Figure 3.9(a)).

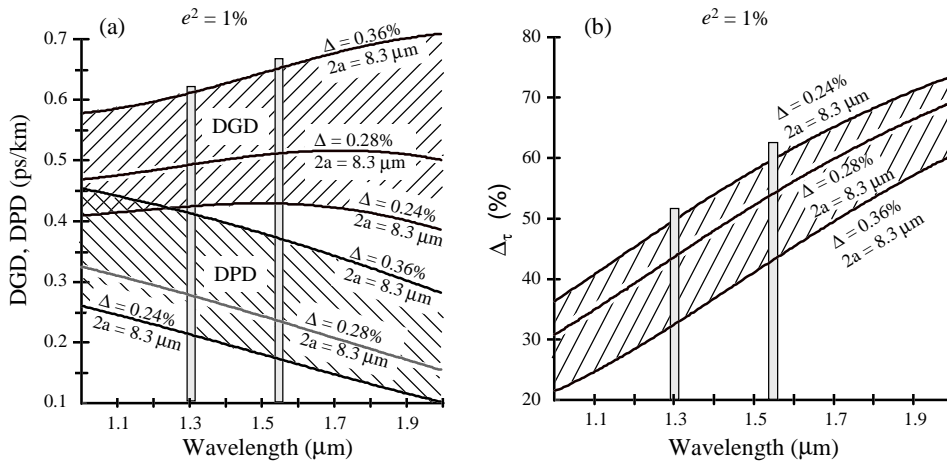


Figure 3.15 Figure 3.15 S-SMF with variation in Δ and core radius (a) DGD and DPD due to $\delta\beta_G + \delta\beta_S$ for different core ellipticities (b) relative difference in DGD and DPD.

Another interesting point appears by comparing the difference of the DGD and DPD for the DSF in Figure 3.16(b) with the one for the S-SMF in Figure 3.14(b), the offset is for both, luckily, around 50% which we will compare with measurements of DGD and DPD on different fibres in Chapter 7.

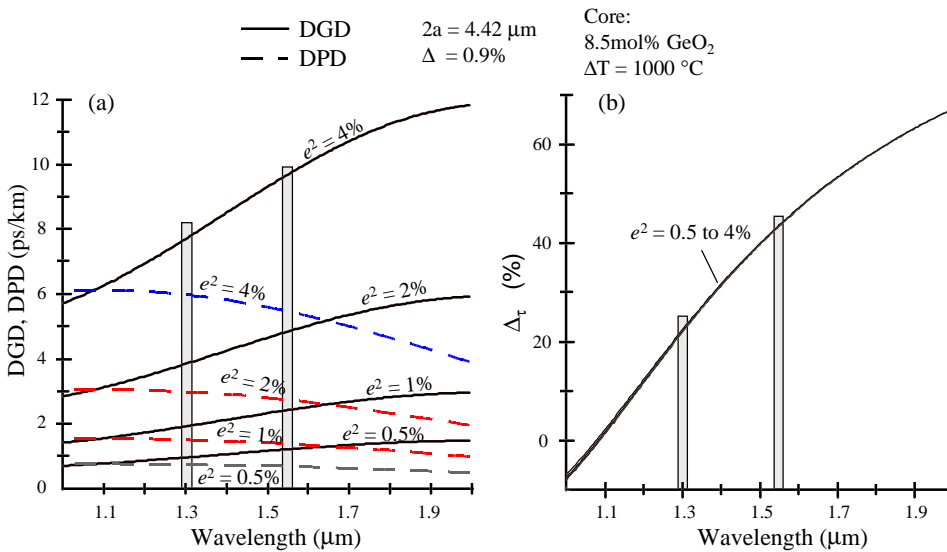


Figure 3.16 Step index DSF (a) DGD and DPD due to $\delta\beta_G + \delta\beta_S$ for different core ellipticities (b) relative difference in DGD and DPD.

In all the above simulations the shape and stress birefringence, wavelength dependence of the stress optic constant and the refractive index have all been taken into account. If these factors are not considered the error introduced is $< 5\%$ in the above simulations. Simulations have further shown that if the electric field distribution is ignored in the stress birefringence, as

given in Equation (3.29) i.e. $b_n(\lambda) = \text{constant}$, the maximum error introduced is <20% for $1 \mu\text{m} < \lambda < 2 \mu\text{m}$ which shows that the stress birefringence does not depend as much on the profile as the shape birefringence.

3.3.2.4 Birefringence and DGD for fibres with different doping structure and different profiles

As mentioned above some fibre manufacturers are also using doping in the cladding e.g. to get a matched cladding step index profile. The use of P_2O_5 and Fluorine in the cladding, as used by BT Labs, makes the thermal expansion coefficient difference in Equation (3.29) smaller, and at some doping level inverts the sign so that $\delta\beta_G$ and $\delta\beta_S$ are in opposition, i.e. their fast axes are orthogonal. The two birefringence effects thus can cancel partially and fibre with low birefringence and low PMD can be designed. Low intrinsic linear birefringence fibre manufacturing techniques were reported in [102] and [103] by preserving the geometrical circularity of the fibre cross section and selecting the dopant materials so that the thermal stresses are minimised. Beat lengths larger than 100 metres have been achieved using this way [103], although in practice this is quite difficult to achieve because of the accurate control of the dopant level required to get zero birefringence. Simulations of the net birefringence and the resultant DGD for S-SMF with doped cladding using 1 mol% and 2 mol% P_2O_5 are shown in Appendix B, where it can be seen that between these two doping levels a change in the direction of the fast axis occurs due to the sign change in the difference of the thermal expansion coefficient.

For more complicated profiles, such as the segmented DSF from Corning or fibre profiles shown in Figure 3.10, stress could originate in the fibre cladding, in this case a finite-element method, which incorporates the material properties and drawing parameters, is the most accurate way to evaluate the stress induced birefringence [81]. Multiple perturbations may be present in fibres simultaneously, such as stress due to core-cladding concentricity, ellipticity in the cladding and or in the segmented core as used in DSF. For multiple perturbations, the total birefringence is the vector summation of the local birefringences as indicated in Equation (3.21).

3.3.2.5 Temperature dependence of $\delta\beta$ and the DGD

The birefringence and DGD in a fibre can change with temperature due to different effects, which can cause problems in sensor applications [84] and fluctuation in the PMD in telecommunication systems [8]. The two main effects are: First, the temperature dependence

of the internal stress birefringence which is mainly due to linear dependence of the thermal expansion coefficient with temperature [101] given in Equation (3.29), whereas it was shown that the temperature dependence of the stress optic coefficient makes a small contribution to $\delta\beta_s$ [84]. Second, the thermal expansion coefficient of coating and buffering material may introduce some perturbation (mode coupling), e.g. for fibre wound with tension on a spool [96], and reduce the DGD randomly. There are also some small temperature effects such as the length increase of the fibre with temperature which, for a 1 km length of fibre, is around one centimetre for an increase in temperature of 20°C. There is also a change in refractive index with temperature which is of the order of $\delta n/\delta T = 1.1 \cdot 10^{-5} / ^\circ\text{C}$ [104]. However, because only the difference in the core-cladding refractive index influences the shape birefringence, $\delta\beta_G$ can be considered as temperature independent.

3.3.3 External transverse stress

Applying an external force to a fibre introduces birefringence with the fast axis in the direction of the applied pressure [78]. The refractive index change can be considered uniform throughout the region of core and adjacent cladding so that for V values larger than one the electric field will be well confined to the core region and the birefringence introduced by the external pressure can be written by a mode field independent equation, [36], [78], [99]

$$\delta\beta_s = \frac{4C}{\pi} \frac{f}{r} k_0 = \frac{8C}{\lambda_0} \frac{f}{r} \quad (3.31)$$

where f is the applied force in N/m^{-1} and r is the outer radius of the fibre. Equation (3.31) applies to sharp concentrated line force to the core centre. For forces distributed over the fibre a reduction of up to a factor of $8/\pi$ may result [78].

3.3.4 Circular birefringence $\delta\beta_C$ effects

Elastic twisting of a fibre in the cold condition causes two effects in the fibre. The first is a geometrical effect which acts to rotate the linear birefringent axes of the fibre with the twist rate, and the second produces torsional stresses which, by the photo-elastic effect, causes circular birefringence $\delta\beta_C$. This optical activity may be defined in the following way: a material is said to possess optical activity if the difference from the launched to the emerged SOP is only in the azimuth, and the ellipticity is constant. Circular birefringence is proportional to the twist rate γ [37], [78]

$$\delta\beta_c = g\gamma = -n^2 p_{44}\gamma = -\frac{2RC}{n}\gamma \quad (3.32)$$

where $g \approx 0.14$ at $\lambda = 1.55 \mu\text{m}$ for typical fibres [37], [105], $p_{44} = (p_{11} - p_{12})/2$ and $R = E/(2(1+\nu_p))$ is the rigidity modulus. According to our experience, the values of elastic twist expected in standard fibres after unwinding from the shipping bobbins is about 0.2 turns/m on average, but we have seen up to 0.4 turns/m of twist in some fibres. Although Barlow [106] showed that circular birefringence can introduce DGD as early as in 1981 it has been ignored afterwards quite often, and in a recent patent [107] it is written “*Twisting the optical fibres at a rate of between two and four twists per meter gives optimum PMD reduction. Additional twisting does not provide substantially more PMD improvement as an upper limit is reached where PMD is no longer sensitive to additional twisting*”. One reason for this may be the lack of a complete analytical equation considering both the circular and linear birefringence simultaneously in the fibre [79]. Many papers in the past have treated the linear birefringence reduction with twist but have neglected the circular birefringence [108], [109]. In Chapter 5 equations governing the DGD for fibre with linear birefringence and elastic twist will be derived and in Chapter 6 the measurement of the DGD on different fibres as a function of twist will be shown.

3.3.5 Spun fibre

Spun fibre exhibiting low net birefringence and low PMD has recently emerged in the commercial market [13], driven mainly as a result of the high PMD values measured in DSF. These spun fibres as patented in Reference [13] from e.g. Lycom Fibre, Denmark (AT&T), contain an alternating rotational spin produced by applying a torque to the fibre during drawing as shown in Figure 3.17. The torque is transmitted back into the neckdown region of the pulling furnace by an oscillation of the pulley wheel in either a horizontal movement of the wheel or by tilting the wheel, so that the fibre is made to rotate across the surface of the wheel and the variation of the spin gets impressed into the fibre. However, it has been known for some time that fibre with low overall birefringence and PMD can be produced by rapidly spinning the preform while pulling the fibre [106], [110], [111], although at this time the spun fibre has been

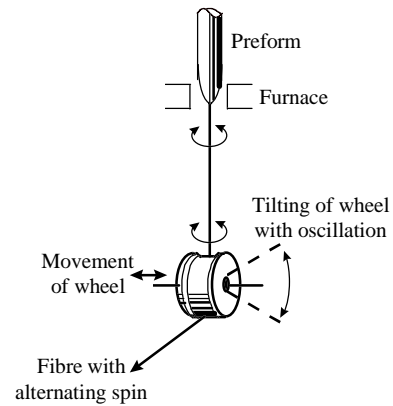


Figure 3.17 Schematic diagram of spun fibre manufacturing with sinusoidal spin.

manufactured using an uniform spin in one direction. Similarly to the elastically twisted fibre, spinning the fibre periodically interchanges the fast and slow axes along the fibre which leads to very low net birefringence, due to compensation of the relative phase delay between the polarisation eigenmodes along the fibre. Spinning the fibre does not introduce circular birefringence because the fibre material is molten so that a permanent spin is being frozen into the fibre with no shear stress giving $\delta\beta_c = 0$ in Equation (3.32). In Chapter 6 the sensitivity of spun fibre to external twist, which always exists to some degree along a fibre, will be investigated and analysed.

When twisting the fibre with large elastic twist (e.g. > 20 turns/m) the temperature dependence of the stress optic coefficient has to be considered [84]. On the other hand spun fibre seems not only to have a low PMD but is also quite insensitive to temperature changes [106].

3.3.6 Birefringence and DGD in erbium doped fibre

A first limitation due to PMD in optical bandwidth is given by the internal PMD in fibres as discussed above. Additional PMD is caused by various optical components in a system such as optical isolators, filters and EDFAs. With the advent of TAT12, PMD was seen as a limitation to transmission bandwidth and was minimised as far as possible not only in the fibre itself but also in the many EDFAs employed. First reported PMD measurements on EDFAs themselves are shown in Reference [18]. In Chapter 6 it will be shown that some of the earliest EDFAs can exhibit PMD values equivalent to a few hundred kilometres of fibre. There are a few reasons for the higher PMD in EDFAs which will be briefly mentioned here. One reason seems to be the use of Al_2O_3 as a codopant in EDFAs (~ 1 to 3 mol% is used in EDF to flatten the gain) which not only introduces a higher thermal expansion coefficient to the fibre core (Table 3.1), but also seems to degenerate the refractive index profile of the fibre using the solution-doping technique [112]. The refractive index profile measured from EDFs are shown in Appendix C. Some other reasons are the smaller core diameter of EDF compared to step index fibre, higher doping level of the core with GeO_2 (~ 8 mol% similar to DSF) and higher core ellipticity compared to standard fibres (see Appendix C).

Dispersion shifted distributed erbium doped fibres (DEDFs) are basically designed for ultra-high bit-rate (≥ 40 Gbits/s) long-haul soliton communication systems [113]. At such bit-rates very short pulses have to be used which leads to short soliton periods and hence short EDFA spacing. DEDF can form a nearly lossless optical pipe and ameliorate the trend towards

shrinking amplifier spacing as the bit-rate is increased in soliton systems, using lumped erbium doped fibre amplifiers. An important potential attraction of soliton transmission is that solitons are more robust against PMD than linear NRZ transmission systems [114]-[116]. PMD can be compensated by a soliton trapping effect where orthogonally polarised solitons can trap each other in the time domain by shifting their frequencies due to an interplay in self-phase modulation and cross phase modulation [114]-[116]. However, this does not mean that ultra-high bit-rate long-haul soliton systems can tolerate arbitrarily large amounts of PMD. A numerical simulation [116] gives an approximation for the range of benign PMD value for such links as

$$PMD \leq 0.3D^{1/2} \quad (3.33)$$

where the PMD and the chromatic dispersion coefficient D , are both in their usual units (ps/\sqrt{km} and $ps/nm \cdot km$). In ultra-high bit-rate long-haul soliton systems, D normally has to be no higher than ~ 0.1 ps/nm•km in order to achieve an acceptably large soliton period (e.g. ≥ 50 km). At this low value of D , Equation (3.33) then leads to the requirement that the PMD of DEDF should be lower than ~ 0.1 ps/ \sqrt{km} . In Chapter 6 measurement results will be shown for the DGD in DEDFs, which by comparing with the expected PMD value in long lengths of fibre (expected mode coupling length in straight cables) seems to be an order of magnitude higher than the above calculated maximum allowed PMD value [117], [118].

Simulations have shown [119] that for NRZ IM pulses in long lengths of fibre (5000 km with low input powers ~ 1 mW), the Kerr effect also seems to be able to compensate partially for PMD in the presence of chromatic dispersion. [119]

3.3.7 Other linear birefringence effects

Further linear birefringence effects are caused by bending [36], [78], the electro-optic Kerr effect from a transverse electric field (very small for silica fibres [78]), and the magneto-optic Faraday effect from a longitudinal magnetic field along the fibre. The latter introduces a non-reciprocal circular birefringence proportional to the axial magnetic field [37], and can be used in current sensors and is exploited in isolators. The bend birefringence with fast axis in the plane of bend is given by [78]

$$\delta\beta_L = 0.5CkE \frac{r^2}{R^2} \quad (3.34)$$

where r is the outer radius of the fibre and R is the radius of bending. Moreover, the bend birefringence will be larger if wound under tension [78], e.g. a fibre wound tightly on a bobbin. Often fibre spooled on a bobbin may cross itself at random distances and this acts as a source of random mode coupling to the internal modes which is likely to be more significant than the introduced additional birefringence [120].

3.3.8 Screening optical fibres for core ellipticity

In Appendix C we have used three different methods to analyse core ellipticity. The first method was carried out in house, using an electron microscope to reveal the fibre index structure. This could roughly resolve only ellipticities above about 5%. A far field scan was carried out at NPL for one fibre sample, a method often used in other references to determine the core ellipticity [70] with an accuracy of 2%. The third method involved screening the fibre preform for ellipticity which was carried out for the fibres manufactured at BT Labs.

3.4 Introduction to PMD

In this section PMD as observed in long lengths of fibre will be examined in the time domain where we introduce the mode coupling length and the principal states of polarisation (PSP), which was developed by Poole [121]. PMD can be a limit in high bit-rate digital systems [8] [9] and leads to non-linear distortions in analogue systems [10].

So far we have assumed $\delta\beta$ to be independent of length and that the DGD increases linearly with length. In reality, in long length telecommunication fibres there exist sources of mode coupling along the fibre, e.g. stress due to external forces, and the local birefringence vector which is described by its local axes and its magnitude will change randomly along the fibre. We can therefore imagine that the fast and slow axes along such a fibre are varying randomly in orientation and hence the DGD does not accumulate linearly with length, and it is more appropriate to describe the accumulation as a statistical random walk process, whereby the mean DGD increases with square root of distance as predicted from the theory of mode coupling in multi mode fibres [78], [80], and confirmed in many measurements in long lengths of fibres [12], [122].

3.4.1 PMD in the time domain

In Chapter 2 (Equation 2.7) a unitary matrix for a birefringent medium without polarisation dependent loss was introduced which in general depends on length and optical frequency, \mathbf{U}

$= f(l, \omega)$. When \mathbf{U} is independent of l (uniform fibre) two eigenvectors corresponding to the polarisation eigenmodes (PEM) of the fibre can be obtained and determine the axis of the birefringence vector on the Poincaré sphere. A pulse launched solely into one of these eigenmodes remains in that mode and no pulse separation occurs. If equal power is launched in both eigenmodes the greatest pulse distortion occurs, as is indicated in Figure 3.18(a), where the total DGD $\Delta\tau$ at the fibre output is shown to be the time difference between the split pulse. In Figure 3.18(b) the same pulse is launched in a simple fibre model which is a concatenation of fibres, all with the same length and birefringence but with the birefringence axes at random orientation. The pulse can be thought to split at each fibre section in two parts with a higher and lower propagation constant defined by the local polarisation eigenmodes of the fibre section, and a random mode coupling of these modes occurring at the fibre interfaces. The probability of power coupling between the two modes as a function of length depends on the chosen length of the fibre pieces (number of fibre pieces) and the random orientation of the fibre birefringence axes. From coupled-mode theory the average DGD (PMD) along the fibre can be expressed as a function of the short length DGD (ps/km) and a so-called polarisation mode coupling length L_C in the fibre as [123]

$$\langle \Delta\tau \rangle = \frac{d(\delta\beta)}{d\omega} \sqrt{lL_C} \sqrt{1 - \frac{L_C}{2l} (1 - e^{-2l/L_C})} \quad (3.35)$$

For long lengths of fibres $l \gg L_C$ the mean DGD from Equation (3.35) grows with the square root of length

$$\langle \Delta\tau \rangle \propto \frac{d(\delta\beta)}{d\omega} \sqrt{lL_C} \quad (3.36)$$

and for short lengths ($l \ll L_C$) we know from Section 3.3 that the mean DGD grows linearly with length

$$\langle \Delta\tau \rangle = \delta\tau = \frac{d(\delta\beta)}{d\omega} l \quad (3.37)$$

The mode coupling length L_C can be obtained by measuring the PMD at different lengths of the fibre, e.g., by a cutting back of the fibre as carried out in Reference [12] and using a best fit to the measured DGD for Equation (3.35). In Section 6.4 an estimation will be made, based on Equation (3.35) from the short length DGD to the long length PMD using expected mode coupling lengths in optical cables.

The PMD in the time domain as indicated in Figure 3.18(b), for a very short input pulse, can be directly calculated from the received pulse spreading, if it shows a Gaussian envelope and is directly related to twice the mean square deviation of this distribution (i.e. the full width) [124], [125]. The short pulsewidth in Figure 3.18(b) is chosen to be short (with respect to the PMD delay of the fibre), and following from that possesses a broad linewidth which ensures the indicated Gaussian distribution (pulse spreading) at the fibre output in the time domain. The effect of the linewidth (or optical frequencies) on the DGD of the fibre can be better understood in the frequency domain where the principal state of polarisation model is defined which will be treated next.

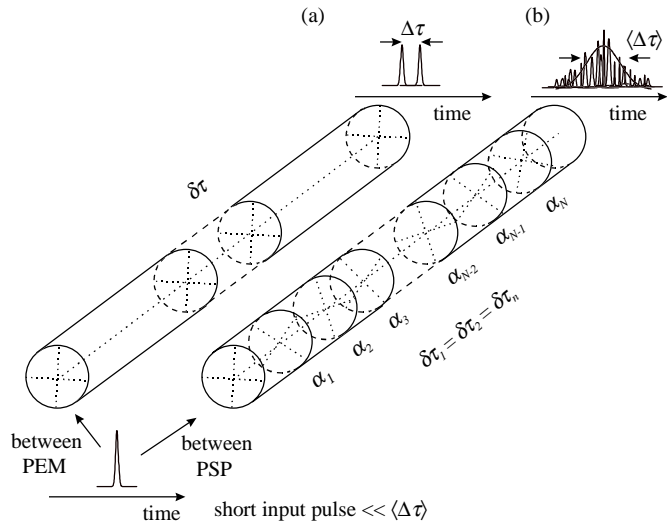


Figure 3.18 Intensity response for short input pulse. In (a) uniform fibre with constant $\delta\beta$ leads to pulse splitting. In (b) fibre with large mode coupling leads to pulse spreading.

3.4.2 PMD in the frequency domain

The output SOP for a uniform birefringent fibre (as e.g. shown in Figure 3.19(a)) as a function of optical frequency makes, in general, only a circular revolution over the Poincaré sphere. In Figure 3.19(a) the output SOP from a HiBi fibre which can be considered to possess uniform birefringence, has been measured at different wavelengths and plotted on the Poincaré sphere. The circular revolution with wavelength change is clearly seen and can be described by a rotation vector, $\vec{\Omega}$, the polarisation dispersion vector [109]. This rotation can be generalised using the Poincaré sphere notation by the following differential equation [37], [126]

$$\frac{d\vec{s}(l, \omega)}{d\omega} = \vec{\Omega}(l, \omega) \times \vec{s}(l, \omega) \quad (3.38)$$

where \vec{s} is the output SOP and $\vec{\Omega}$ corresponds to the positive output PSP which coincide with the PEM in the absence of polarisation mode coupling, in which case the PEM are frequency independent over very broad bandwidths. The importance of the PSP just introduced on the Poincaré sphere arises when the fibre matrix \mathbf{U} depends on l and ω as in long length telecommunication systems which are affected by random birefringence and mode coupling. The PEM description is no longer suitable in connection with experiments in identifying true eigenmodes of the fibre. However, it has been observed and proved theoretically that it is still possible to identify two principal states of polarisation (PSPs) which show no wavelength dependence to first order over a finite wavelength range (Poole and co-workers [121] [126]), although they do not travel unchanged from the fibre input to the output.

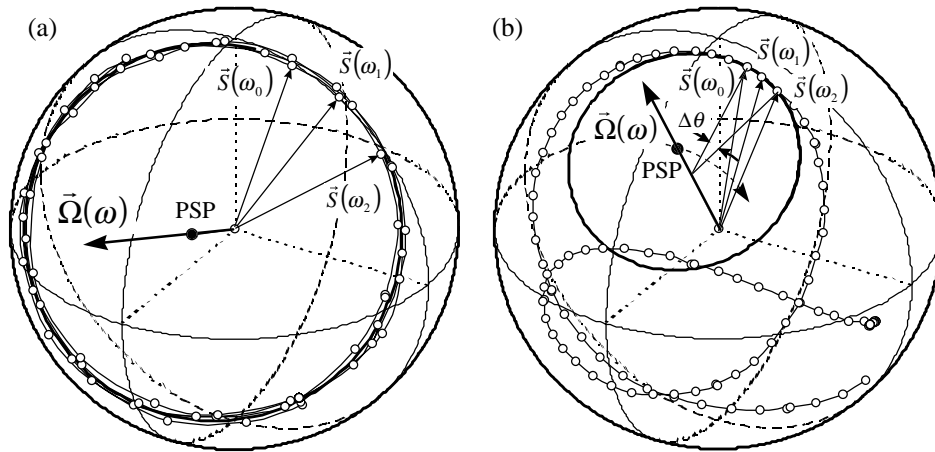


Figure 3.19 Measured output SOP as a function of optical wavelength. In (a) for a 3 m HiBi fibre with $\Delta\lambda = 0.1$ nm from 1550 nm to 1556 nm. In (b) 25 km S-SMF fibre with $\Delta\lambda = 1$ nm from 1485 nm to 1565 nm. The heavy line shows the best fitted arc calculated over a small range of SOPs whose centre gives the direction of one PSP where the second is located diametrically opposite on the sphere.

A typical trace of the output SOP versus wavelength on the Poincaré sphere for a 25 km long DSF wound on a bobbin is shown in Figure 3.19(b), where for a small wavelength range a best-fitted circle can be found whose axes correspond to the first order PSP in the fibre at this wavelength range. The DGD is given by the modulus of the rotation vector $\vec{\Omega}$, which can be calculated from the rotation angle $\Delta\theta$ indicated in Figure 3.19(b) between two frequencies, where the PSP can be considered as constant [11].

$$\Delta\tau = |\vec{\Omega}| = \frac{d\theta}{d\omega} \approx \frac{\Delta\theta}{\Delta\omega} \quad (ps) \quad (3.39)$$

This can, in general, be expressed as the speed of SOP rotation with optical frequency. One of the important property of the PSPs is that if the polarisation state of an input signal coincides with one of the PSP then the minimum system penalty due to PMD is achieved [121]. Figure 3.20 (a) and (b) show a typical DGD plot versus wavelength for a short length of Bow Tie fibre exhibiting a high PMD value and a long length of DSF wound on a bobbin exhibiting a low DGD value.

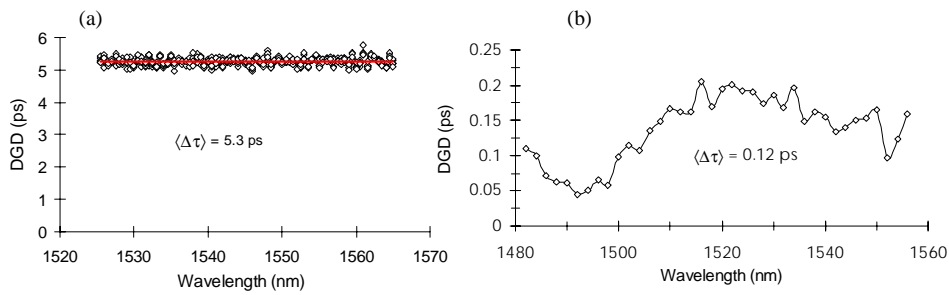


Figure 3.20 DGD versus wavelength (a) in 3 m Bow Tie fibre with basically no mode coupling (b) in ~ 8 km DSF from Corning on shipping bobbin.

The fundamental difference between the PEMs and PSPs is that the PSPs are not explicitly correlated with the local birefringence like the PEMs, but rather depend on the total net effect of the birefringence of the entire fibre length. The general equation describing the evolution of the PSP is expressed by [11]

$$\frac{d\vec{\Omega}(l, \omega)}{dl} = \frac{d(\delta\vec{\beta}(l, \omega))}{d\omega} + \delta\vec{\beta}(l, \omega) \times \vec{\Omega}(l, \omega) \quad (3.40)$$

where $\delta\beta$ represents the local birefringence with the random perturbation which is due to its frequency dependence $(\delta\vec{\beta}(l, \omega))/d\omega$ responsible for the growth of the dispersion in the optical fibre. To obtain the PSP as expected in a standard low birefringent fibre by modelling, the local birefringence could be taken as $\delta\vec{\beta}(l) = \delta\vec{\beta}_0 + \Delta\delta\vec{\beta}(l)$ with $\delta\vec{\beta}_0$ as a constant birefringence, and $\Delta\delta\vec{\beta}(l)$ as a fluctuating random perturbation with uncorrelated Gaussian components [127]. Alternatively, as shown in Figure 3.18(b), a simple random concatenation of short, constant birefringence, fibre pieces is often used [128], [129], with mode coupling

occurring at the junction of any two fibre pieces. Both methods obtain the PSP by an underlying statistical description and simulation. Theory and experiment have shown that for fibre lengths larger than the correlation length L_C , the probability function of the PSP components are three independent equally distributed Gaussian variables [11]. Their combined effect, to give the probability density function of the differential group delay between the output PSP, $\Delta\tau$, is therefore represented by a Maxwellian distribution [11] [130]

$$P(\Delta\tau, l) = \frac{2\Delta\tau^2}{\sqrt{2\pi}q^3} e^{-\Delta\tau^2/2q^2} \quad (3.41)$$

where $q^2 = L_C \delta\tau^2/l$ is the variance with $\delta\tau/l = d(\delta\beta)/d\omega$ the differential group delay per unit length of the unperturbed fibre. The standard deviation and mean value of the DGD is

$$\langle\Delta\tau\rangle = \sqrt{\frac{8}{\pi}} \frac{d(\delta\beta)}{d\omega} \sqrt{L_C l} \quad \text{and} \quad \sigma = \sqrt{\frac{3\pi-8}{\pi}} \frac{d(\delta\beta)}{d\omega} \sqrt{L_C l} \quad (3.42)$$

The mean DGD for fibre length $l \gg L_C$ increases with \sqrt{l} as expected and as observed in many measurements [11], [12], [80], [123], [130],[131]. In Figure 3.21(a), the DGD versus wavelength of a 25 km fibre with high second order PMD (variation of the DGD with wavelength) is shown and in (b), the corresponding histogram shows a fitted Maxwellian distribution. The histogram is close to a Maxwellian distribution due to the low correlation of the DGD values in the measured wavelength range leading to a large number of independent samples.

Equation (3.42) shows that the PMD and standard deviation is directly proportional to the short length DGD, which itself is mainly governed by the intrinsic fibre birefringence. For this reason, it is important to understand the expected intrinsic birefringence in the fibre, and this is mainly investigated in the following chapters for different fibres. In Section 6.4, the expected mean coupling length in cabled fibres will be discussed.

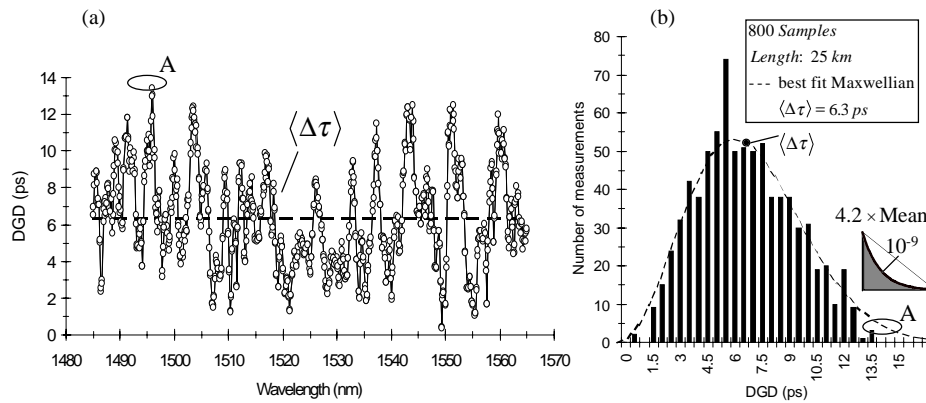


Figure 3.21 In (a) PMD characteristic of 25 km fibre which shows high mean value and strong fluctuation, measurement time ~ 1 hour with one repetition. In (b) histogram of the DGD values with best fitted Maxwellian, (measurement carried out at BT Labs).

We can conclude from above that in the long length regime the PMD in the time domain is obtained directly by the mean square deviation of the distribution which arrives basically from the theory of modal dispersion in multi mode fibres and for that reason we speak of mode coupling in the time domain. In the frequency domain, the PMD for a long length regime is simply the mean DGD, which can be obtained as an average over a large wavelength range (Figure 3.21), or as the average at a single wavelength over a large range of environmental fluctuations. In the frequency domain, we can also consider second order PMD which will be further discussed in Section 3.5. Both the time and frequency domain methods seem to be equivalent and give comparable PMD values when a suitable conversion factor is used [14], [124] [132]-[134].

3.5 Measurement methods for PMD

PMD can be measured in the time domain or in the frequency domain but in principle all the measurement methods which will be discussed below rely basically on the frequency dependence of the output SOP relative to a fixed input SOP.

In the time domain, we could measure the PMD directly from the pulse spreading, as shown in Figure 3.18, by using a short pulse. However, this suffers from two major draw backs; at short lengths we would have to insert equal powers into the two PEMs (PSP) to get the maximum spreading, and at long lengths we would need very short pulses and a fast receiver

(fs resolution) in order to see the Gaussian distribution. In reality, some kind of interferometric method is often used in combination with a low coherence light source, e.g. an LED. A typical interferometric set-up for measuring PMD is shown in Figure 3.22(a).

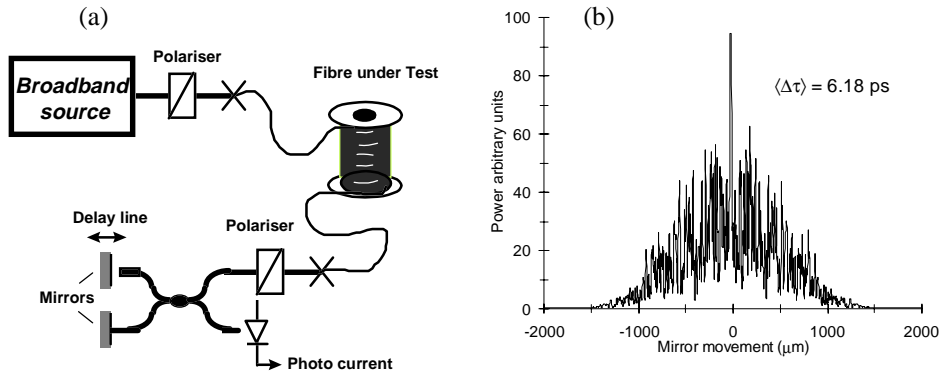


Figure 3.22 Measurement of PMD using interferometric technique (a) Michelson interferometer with fibre coupler (b) PMD in 25 km long length of fibre measured with GAP interferometer, measurement is taken at the same fibre as shown in Figure 3.21, (measured at BT Labs).

The output light is polarised by a linear polariser and split into two paths where one path can be delayed and after recombination is detected by a photodiode. The measured photocurrent shows coherent fringes as shown in Figure 3.22(b) whenever the DGD of the fibre or device under test is compensated by the differential delay introduced in the interferometer. For a long length of fibre, the envelope of the measured current shows a Gaussian distribution [135] (neglecting the centre peak) and the PMD is determined by the variance of the Gaussian fit multiplied by some factor [124].

In the frequency domain, the most often used technique is the polarimetric method in combination with a tunable wavelength source. Another common method is the wavelength scanning method which simply counts the measured power extrema through a fixed analyser at the output of the fibre as a function of frequency. From that, the mean DGD of the fibre can be calculated [129]. For the polarimetric PMD method, the set-up is shown in Figure 3.23. The source is swept through the wavelength range of interest and the output SOP for three different input SOPs (e.g. linear polariser at 0° , 60° and 120°) is recorded for each wavelength.

There are now different possibilities for obtaining the PMD by using the polarimetric method but all use the principal state of polarisation concept. One method we have already mentioned

in the section above simply measures the arc of the output SOP over a small wavelength range (see Figure 3.19).

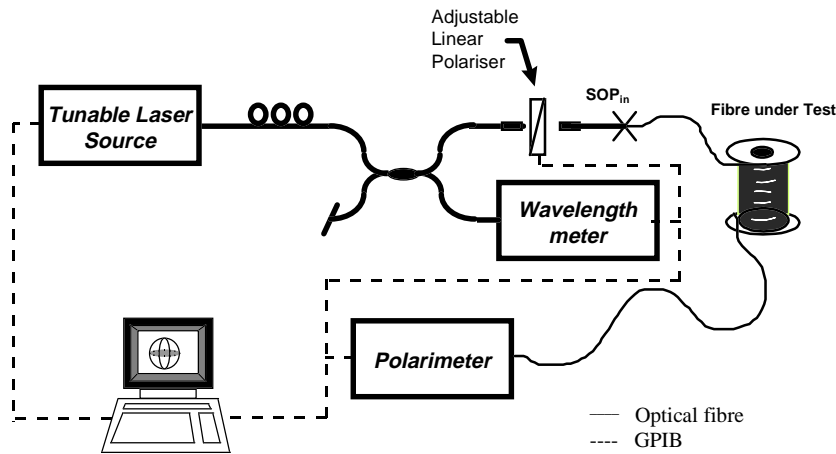


Figure 3.23 Experimental PMD measurement set-up.

One big drawback of this method is that if the output SOP is close to a PSP, the arc radius is small and in the presence of noise it is difficult to fit the arc on the sphere with good accuracy. A way around this problem would be to use two input SOPs, e.g. at 0° and 45° , which leads basically to the method most commonly used in connection with a polarimeter, which is the Jones matrix eigenanalysis (JME). JME can determine the fibre transfer matrix to within a complex constant by using only linearly polarised input SOPs [136] and has been used to determine the DGD from the eigenvalues of the obtained matrices at different wavelengths by Heffner [137]. JME is the most commonly applied polarimetric method for determining the DGD because of its high accuracy of typically ± 1 fs, although attosecond resolution was obtained in Reference [138]. Another method which is basically equivalent to the JME will be shown in Chapter 5 where the full Mueller matrices at different wavelengths are obtained using three input SOPs. However, one SOP has to be elliptical, (e.g. right or left circular). This makes the method worse in practice because of the less accurate elliptical SOP generation and the wavelength dependence of the waveplate used to generate the SOP.

A comparison of the different measurement methods in theory and measurement, e.g. round robin measurement, can be found in many papers [14], [124] [132], [133]. This shows the equivalence of the PMD value obtained in the time and frequency domain, as is also shown by comparing the PMD value in Figure 3.21(b) obtained from the polarimetric method with the PMD in Figure 3.22(b) obtained from the interferometric method for the same fibre. Each method has its advantages and disadvantages. The advantage of the time domain is that it directly gives the mean value of the distribution from the most natural means, making it fast

in measurement time when compared to the polarimetric method where the statistic in the frequency domain has to be obtained by independent measurements, either over a broad wavelength range and/or at different measurement times. On the other hand, it has been shown by theory and simulation [125] that the interferometric method with strong mode coupling, can show an unwanted dependence on the LED characteristics. Although the polarimetric method is the most expensive set-up (tunable wavelength source and polarimeter) in understanding the fibre properties, it has some outstanding distinctions over the other methods. It includes high accuracy for measuring short lengths of fibres (Chapter 6) providing wavelength resolved measurements of the DGD and measuring the movement of the PSPs with wavelength (important when considering second order PMD).

3.6 Measured PMD in short and long fibre lengths

In this section, JME measurements will be revisited and the relation between first and second order PMD introduced. It will be shown that a large second order PMD is basically the mechanism which causes the DGD to show a Maxwellian distribution. At the end of this section, the problems with PMD compensation will be discussed.

3.6.1 First order PMD

A typical DGD measurement in a short length of fibre (linear DGD regime) is shown in Figure 3.20(a) where we used a HiBi fibre to demonstrate the first order wavelength independence of the PSP on the Poincaré sphere. Furthermore Figure 3.20(a) shows a high DGD value which is constant over the considered wavelength range. This would be expected because, as for the external applied stress birefringence in Equation (3.31), the birefringence can be considered to be independent of the mode field and just proportional to the optical wavelength. The DGD values can be said to be highly correlated with each other over the whole wavelength range, the PSP correspond to well defined symmetry axes and the DGD is deterministic. Similarly, the DGD values for short sections of low birefringent fibre with no random mode coupling show a flat trace for the DGD versus wavelength (apart from some curvature do to the shape birefringence) but the DGD is much lower compared to the HiBi fibre (measurements are shown in Chapter 6).

DGD measurements for increasing lengths of different fibres wound on fibre bobbins are shown in Figure 3.20(b) and Figure 3.24(a) and (b). At first, it can be seen that the general trend is towards higher mean DGD values for increasing fibre lengths. Although these are different fibres independently measured because the distance differences are quite large this trend can still be clearly seen.

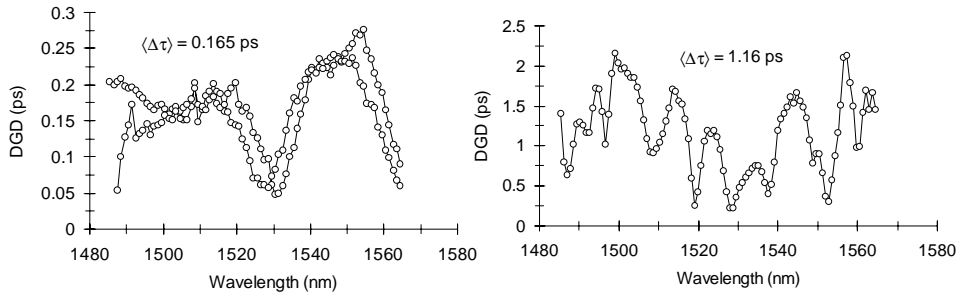


Figure 3.24 DGD versus wavelength for (a) 25 km S-SMF on shipping bobbin and (b) 100 km DS fibre on 6 concatenated shipping bobbins.

Furthermore, including Figure 3.21(a) into the comparison, suggests a relationship between the average PMD of a fibre and the rate of change of the DGD with wavelength. For example, in Figure 3.20(b), the mean DGD is low and the rate of change with wavelength is also low. In Figure 3.21(a), the mean DGD value is high and the rate of change with wavelength is also high. It is interesting to note that this relationship is not due to a change in mode coupling because this should be high for all the fibres in the above figures as they are all wound on bobbins. The DGD values in Figure 3.21(a) are from two consecutive measurements (measurement time ~ 1 hour) and show a high stability with time but a low correlation for even small frequency differences, giving a good Maxwellian distribution in the histogram of Figure 3.21(b). For fibres spooled onto a shipping bobbin, as shown in Figure 3.20(b) or in Figure 3.24(a) which show low mean DGD, even consecutive measurements over a couple of hours gives a poor statistical distribution of the measured DGDs over wavelength and time, indicating a high to medium correlation of the DGD values.

3.6.2 Second order polarisation mode dispersion

Second order PMD leads to an effective differential chromatic dispersion of the two polarisation modes and can cause depolarisation as for example in Figure 3.18(b) where the output signal is a set of unpolarised pulses caused by pulse spreading. For a fibre with no random mode coupling but $\beta_x'' \neq \beta_y''$, the second order PMD can be calculated by

substituting the first order DGD given in Equation (3.18) for constant PSP into Equation (3.12)

$$\frac{1}{l} \frac{d(\delta\tau)}{d\lambda} = \frac{2\pi c}{\lambda^2} \left(\frac{d^2(\beta_x)}{d\omega^2} - \frac{d^2(\beta_y)}{d\omega^2} \right) \approx \frac{1}{l} \frac{\Delta\tau}{\Delta\lambda} \quad \left(\frac{ps}{nm \cdot km} \right) \quad (3.43)$$

The second order PMD for constant PSP as simulated in Section 3.2 is very small as can be directly visualised by just considering the slope of the DGDs in the different figures (see e.g. Figure 3.14), and can, in general, be neglected in elliptical fibres. A different picture is if random mode coupling acts on the fibre and the fibre still shows a high mean DGD value, e.g. the fibre shown in Figure 3.21. Now the slope $\Delta\tau/\Delta\lambda$ is much larger over a small wavelength range. Second order PMD arises basically due to the movement of the PSP and this movement with optical frequency has now also to be considered in Equation (3.43). The model of the first order dispersion vector has to be extended to allow the dispersion vector to depend on wavelength which can be carried out by expanding $\vec{\Omega}(l, \omega)$ into a Taylor series about the centre frequency ω_0

$$\vec{\Omega}(l, \omega) \approx \vec{\Omega}(l, \omega_0) + \vec{\Omega}'(l, \omega_0) \Delta\omega + \dots \quad (3.44)$$

where $\Delta\omega = (\omega - \omega_0)$ which can be re-written considering only first and second order PMD

$$\vec{\Omega}(l, \omega) = \Delta\tau \hat{\Omega} + \frac{d(\Delta\tau)}{d\omega} \hat{\Omega} \Delta\omega + \Delta\tau \frac{d(\hat{\Omega})}{d\omega} \Delta\omega \quad (3.45)$$

where the derivatives are taken at the frequency ω_0 . The first term of Equation (3.45) shows the first order PMD with constant PSP, the second term quantifies basically the same as given in Equation (3.43), and the third term gives the frequency dependence of the PSP. In [127], the statistical characteristics of first and second order PMD were analysed and in [139], it was shown that the bandwidth associated with the movement of the PSP on the Poincaré sphere is inversely proportional to the first order PMD as already suggested from the observed higher fluctuation for higher mean DGD values (compare Figure 3.21 with Figure 3.20(b)). After Reference [139], second order PMD in a 10 Gbit/s transmission systems seems to severely compound first order PMD for mean DGD values larger than 5 ps in the presence of large chromatic dispersion, but after [140], recent measurement results suggest

that second order PMD is not a serious problem in fibres with mean DGD values less than the maximum allowed first order PMD, (see Section 6.5 for maximum allowed first order PMD values). This seems to indicate that more work on the impact of second order PMD on the transmission bandwidth has yet to be carried out.

3.6.3 Depolarisation due to first and second order PMD

First order PMD can depolarise the transmitted light pulse if the delay between the transit time of the two orthogonal modes becomes greater than the coherence time of the source [141]. If the state of polarisation of the input signal coincides with one of the PEM, no depolarisation occurs in short lengths of fibres. In long lengths of fibres where the PSP definition is valid, the same is true. Minimum depolarisation to first order is obtained if the input SOP coincides with one of the PSP which also gives the minimum penalty due to polarisation mode dispersion. Another aspect is the depolarisation of the transmitted light pulse due to second order PMD. Second order PMD has not only the effect of a differential chromatic dispersion between the two PSP but also can cause depolarisation as in the case of the short pulse shown in Figure 3.18(b), whose coherence length can be assumed to be equal to the pulse width (low coherence), and the received spread pulse consists of a set of completely unpolarised pulses [8]. For pulse splitting, on the other hand, as shown in Figure 3.18(a), the two pulses remain polarised if the first order PMD is smaller than the pulse coherence length. Pulse splitting will also be observed in the fibre with random mode coupling shown in Figure 3.18(b), when using a longer pulse (lower frequency Fourier components in the pulse, larger coherence length) and the split pulses are still polarised.

3.6.4 PMD compensation techniques

PMD compensation is a difficult task in real systems because the output SOP and PMD fluctuation is of a statistical nature and varies with temperature and time due to fibre handling [142]-[144]. In general, it can be said that while various schemes of chromatic dispersion have been proposed [5], currently there is no simple and cost effective optical or electrical compensation for PMD, mainly because polarisation control requires an active component [145]-[147].